

Green & Clean Al-Cu alloys

by

Qingyu Pan

A Thesis

Submitted to the Faculty

of the

WORCESTER POLYTECHNIC INSTITUTE

in partial fulfillment of the requirements for the

Degree of Master of Science

in

Material Science & Engineering

December 2018

APPROVED:

Dr. Diran Apelian, **Major Advisor**

Dr. Richard Sisson, **Head of Department**

Abstract

For aluminum alloy casting, degassing is a necessary step for molten metal, which can extract the dissolved hydrogen in the melt. For copper-containing aluminum alloys, a traditional method is that using mixed gas of inert gas and chlorine as degassing agent. Because of the toxicity of the gaseous chlorine, the industrial is trying to avoid using it even though this method can contribute to good castings. As a potential solution, the foundry only used argon during degassing, however, the castings with this method were unacceptable since the occurrence of defects.

The goal of this project is to develop a new green and clean degassing method for copper-containing alloys without the usage of gaseous chlorine. To achieve this goal, identify those defects and figure out the source of those defects are necessary. Totally four hypotheses of the occurrence of defects were supposed and two of them were discussed in this thesis. They are ineffective hydrogen removal and metal-mold reaction. Experiments were set in WPI and Palmer Foundry to investigate defects from samples with different conditions. This thesis collected and discussed the results from experiments, and made the conclusion that whether these two hypotheses contribute to the occurrence of defects.

Acknowledgement

I would like to express my deepest and sincere gratitude to following people who gave me help in various ways during this two years in WPI.

First, my greatest appreciation to Professor. Diran Apelian, my thesis advisor. He gave me amounts of invaluable suggestions not only on this project but more on my life and courses. He taught me how to make a good presentation. He encouraged me to improve my language and to communicate with others. He supported me in every way. It is my pleasure to work with him in ACRC.

My sincere gratitude to Dr. Carl Soderhjelm. He has always been available for me and patient in helping me solve kinds of problems. Thanks to challenges he set for me, which let me grow up. Thanks to kinds of advices he gave me, which made my thesis and presentation prettier. And also thanks to his encouragement on my work.

I would like to send my special thanks to Alino Te for giving me kinds of help and answering my kinds of questions. I am so lucky to sit next to him.

A special thanks to our focus group members, Brian Began, David Weiss and Jim Lagrant for supporting our project and providing us help and suggestions.

I would like to give my gratitude to my colleagues in ACRC, Libo Wang, Eunkyung Lee, Ning Sun, Audrey Jean-Philippe, Jeremy Fedors, Yangyang Fan, Richard Eberheim, Mohammad Asadikiya and Songge Yang. I appreciate the time that working with you.

I also thank Maureen Plunkett, Michael Collins, Carol Garofoli and Renee Brodeur for their assistance in my work and my experiments.

Ultimately, I owe my deepest gratitude to my family, my parents. Thank you for your support all the time.

Table of contents

1. Introduction.....	1
2. Problem Statement	4
3. Hypothesis.....	5
4. Approach.....	6
5. Experimental method	8
5.1. Hydrogen extraction	8
5.1.1. Experimental steps	8
5.2. Metal-Mold Reaction	12
5.2.1. WPI Trial	12
5.2.2. Palmer Trials	17
6. Results and discussion	24
6.1. Effectiveness of hydrogen extraction	24
6.2. Internal defects	29
6.2.1. Chemical composition	29
6.2.2. Degassing effectiveness	30
6.2.3. Mechanical properties.....	31
6.2.4. Fracture surface.....	40
6.2.5. Fluidity.....	47
6.3. Surface defects	48
7. Conclusion	53
Reference:.....	54

1. Introduction

Aluminum and aluminum alloys are widely used in various fields because of their unique combination of properties, and their consumption is second only to that of steel in the world ^[1]. So that it is important to avoid the influence of defects on the quality of aluminum alloys products. Porosity as a main defect can deteriorate the mechanical properties of castings. Basically, there are two types of porosity in castings, one originates from the gas that has dissolved in the melt and the other one originates from shrinkage. For aluminum alloys, hydrogen is considered as the only gas that can be dissolved in the melt ^[2]. It is true that under special conditions, nitrogen can also dissolve in the melt, however, it is uncommon in ordinary aluminum alloy castings. Figure 1.1 shows the assessed phase diagram of aluminum and nitrogen ^[3]. It can be seen that only small amounts of nitrogen start to dissolve in the melt when the temperature is above 1500°C. Ordinarily, the nitrogen in the aluminum alloy is formed as aluminum nitride (AlN) instead of gas porosity.

The hydrogen can form porosity because of its different solubility under different temperatures. Figure 1.2 shows the variation of hydrogen solubility with changing melt temperatures ^[4]. The solubility of hydrogen in the aluminum alloy melt decreases as temperature decreases, and it drops dramatically at the melting point. Hence, when the aluminum alloy solidifies, there are amounts of atomic hydrogen that cannot escape from the melt and form molecular hydrogen, creating porosity in the castings. Unfortunately, it is difficult to avoid hydrogen entering the melt since it mostly originates from the water vapor in the atmosphere. Thus, melt treatment is necessary to eliminate the dissolved hydrogen for the manufacture of castings with better quality. Generally, degassing is used before the casting process to extract the hydrogen. Several degassing methods include rotary impeller degassing, vacuum degassing, ultrasonic degassing and tablet degassing using hexachloroethane (C₂Cl₆) are commonly employed ^[5]. Currently, rotary impeller degassing is widely applied in industrial fields due to its higher efficiency ^[6]. During degassing, the inert gas or a combination of the inert gas and reactive gas are purged into the melt from the rotary impeller. Since the partial pressure of hydrogen is lower in the purged gas bubble than the melt, the hydrogen can be extracted into the bubble and transferred to the melt's surface ^[7]. Normally, with rotary degassing, the hydrogen content in the melt can be reduced to 0.10cm³/100g Al in some critical industrial fields ^[8].

For copper containing aluminum alloys (the copper content is above 1 wt. %), which combine higher

strength and higher hardness, gaseous chlorine mixed with argon is commonly used for degassing in the industrial foundry. At present, manufacturers try to minimize the usage of chlorine due to its toxicity. The gaseous chlorine can cause chest pain when the concentration is over 60 ppm, and over 1000 ppm could cause death. It has been verified that argon degassing without chlorine can efficiently remove the hydrogen from the Al-Si alloy melt ^[9]. Therefore, if this similar method can be applied on copper containing aluminum alloys, it is favorable for the decrease on the consumption of chlorine and improvement on work environment. Nevertheless, argon degassing brings an amount of defects to the surface and inside of copper containing aluminum alloys castings, which are unacceptable.

To develop a novel chlorine free molten metal processing technique, it is necessary to study the origin of the defects and their formation mechanism. Basically, the defects are generated either by contamination from surroundings or imperfect casting procedures. From the nature of the problem, it is believed that the defects have a close correlation with the casting procedure. Based on the analysis on the whole casting process, four possible causes for defects that could happen during casting were proposed: ineffective degassing, ineffective oxide/inclusion removal, oxide generation by turbulence and metal-mold reaction. In this thesis, the experiments with different independent variables were made with the help from Palmer Foundry. Samples with various defects were analyzed, and the possibility of ineffective degassing and metal-mold reaction were mainly discussed.

This thesis is divided into four parts. Part 1 introduces the significance and goal of this project. Part 2 outlines the experimental work including experimental apparatus and steps in more detail. Part 3 shows results from different experiments and the discussion. The conclusions are presented in Part 4.

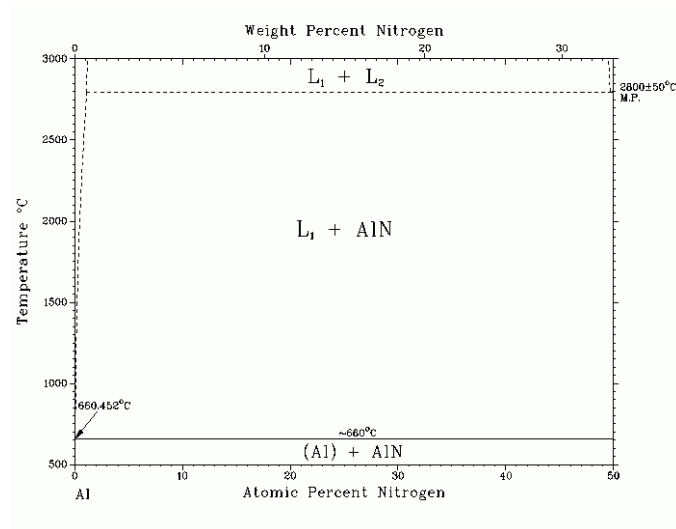


Fig 1.1 The assessed phase diagram of Al-N [3]

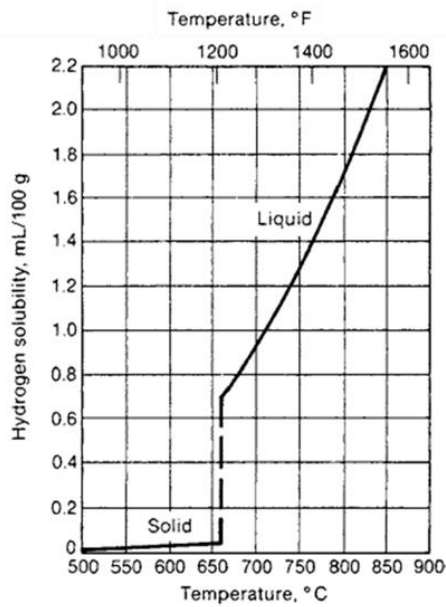


Fig 1.2 Solubility of hydrogen in aluminum at 1 atm hydrogen pressure [4]

2. Problem Statement

Degassing is a necessary cleaning procedure during casting. Unlike silicon-containing aluminum alloys, which can be degassed by the inert gas, copper containing aluminum alloys utilizing inert gas degassing do not exhibit good mechanical properties. However, Cu-containing alloys (the copper content is above 1 wt. %) degassed by chlorine have good mechanical properties. Since chlorine is harmful to the environment and operators, it is necessary to seek for a green and clean solution to clean the molten Cu containing alloy before casting, and a method which does not compromise the mechanical properties of the alloy.

Eck Industries, one of the founder of this project, tried to use argon to replace gaseous chlorine during degassing for Al-Cu alloys, however, it is found that two kinds of defects occur on the castings: surface defects, which can be observed by the naked eye, and the internal defects which can be detected by the CT scan (see Figure 2.1). Hence, it poses a big challenge for the manufacture of Al-Cu alloy casting with good quality. Therefore, it is of significance to get more insight of the origin of defects and formation mechanism during inert gas degassing,

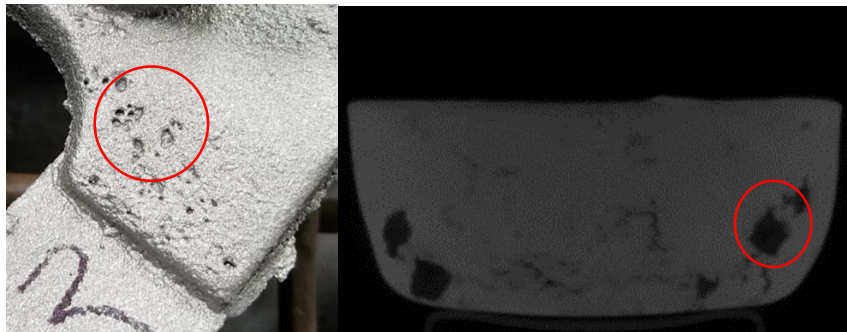


Figure2.1. Different types of defects occur on castings with argon degassing; Left: Surface defects; Right: Internal defects

3. Hypothesis

Defects, which deteriorate the quality of castings could be caused by outside contamination or formed during casting process. Though it is hard to entirely exclude the possibility of exogenous contamination, it is speculated that they are most likely to generate during the casting in this project. Generally, an integral cast process can be divided into four steps, which are melting, transfer, degassing & cleaning and pouring (Figure 3.1). In the first two steps, raw material ingots are selected and melted in the crucible. Any inclusions that exist in ingots or are introduced into the crucible could cause the occurrence of defects at the later stages during casting. Before the melt is poured into molds, it is necessary to extract the hydrogen dissolved in the liquid and inclusions. All these works are included in degassing & cleaning step. Hence, the effectiveness of cleaning procedure contributes to the cleanliness of castings and the number of defects. The pouring step is applied after melt cleaning in which liquid metal is poured from crucible to molds. The first two steps can be controlled during casting process, hence, considering the nature of this problem, the origin of defects should be derived from either degassing & cleaning or pouring steps.



Figure 3.1. The handling process of the aluminum alloy and the proposed four hypotheses.

Four hypotheses are proposed from the last two steps (Figure 3.1). As mentioned above, the effectiveness of degassing & cleaning step influences the final quality of castings. Degassing with inert gas such as argon or the mixed gas such as chlorine with nitrogen can promote the diffusion of dissolved hydrogen in the flux gas bubbles so that hydrogen can be extracted effectively. Any possibility that hydrogen or inclusions cannot be removed entirely could leave porosity and defects in the castings. When the liquid metal is poured into molds, the melt could react with oxygen easily which generates new oxides. Nevertheless, it is difficult to avoid this phenomenon if the gating system is improper. Another hypothesis is the reaction between liquid metal and sand mold, which causes the formation of defects on the surface of castings.

This thesis is focused on the two of these four hypotheses, ineffective degassing and metal-mold reaction.

4. Approach

Based on the proposed hypotheses, two objectives aim to achieve in this thesis: prove the effectiveness of the inert gas degassing for copper containing aluminum alloys; prove if the metal-mold reaction could influence the formation of defects. Two parts of experiments were made to achieve these objectives.

The effectiveness of degassing can be represented by the remaining hydrogen content in different aluminum alloy melt with degassing. A356 and A206 were selected as their different copper content. The hydrogen content in the melt can be measured directly by using Alspek H system during degassing. The variation of hydrogen content with degassing time can be obtained. Also, analysis on castings can show the remaining hydrogen content indirectly. Hence, distribution of porosity inside castings and density statistics were collected in experiments.

The presence of defects on casting surface suggests that the molten aluminum alloy could react with the mold. Thus, the second part of experiments with different independent variables were designed to get the samples with different levels of defects. By comparing those results, it can determine which condition can result in this reaction and the formation of defects. Considering the whole process, three independent variables were selected as follows.

- Alloy type
- Cleaning procedure
- Mold type

Other parameters like melt temperature, cleaning time are set as constant in the experiments.

Two kinds of aluminum alloy, A356 and C355 were used because of their different copper contents. The two molten alloys were degassed by three different ways, argon degassing, argon degassing with flux, chlorine. For comparison, no any cleaning procedures were also processed. It should be noticed that the present work is based on sand casting so the sand type was chosen as another variable. Besides, green sand and no-bake sand, steel mold was also used to prove whether or not there is any reaction between melt and sand.

For safe use of chlorine safely and the high efficiency of experiments, all the trials were made in the laboratory of Worcester Polytechnic Institute (WPI) and Palmer Foundry. They were designed as WPI trials and Palmer trials. The independent variables in different trials are given in Figure 4.1. The WPI trials aim to clarify the effect of cleaning procedures and alloy type on the internal defects,

whereas, In Palmer, no-bake sand mold and green sand mold which cannot be transported were used to disclose the effect of mold type on surface defects.

	WPI trial	Palmer trial
Alloy type	A356 C355	A356 C355
Cleaning procedure	Reference; Argon; Argon with flux	Reference; Chlorine; Argon
Mold	No-bake sand mold Steel mold	No-bake sand mold Green sand mold

Figure 4.1. Independent variables in different trials.

5. Experimental method

5.1. Hydrogen extraction

The designed experiments aim to verify the effectiveness of Ar degassing procedure on copper containing aluminum alloys. Two types of alloys were used, A356, on which Ar degassing has been applied successfully, and A206, which is a significant kind of Al-Cu alloy. Their compositions are given in Table 5.1. Alspek H system was used during degassing so as to monitor the variation of hydrogen content. After cleaning procedure, reduced pressure test (RPT) was performed to evaluate the effectiveness of hydrogen extraction qualitatively. Furthermore, the density of the samples collected from different degassing stages was used to determine the porosity content after cleaning.

Table 5.1. The composition of aluminum alloys used in the trials (wt. %)

Alloy	Si	Cu	Mg	Fe	Ti	Al
A356	6.9	0.02	0.33	0.65	0.05	Bal
A206	0.08	4.6	0.23	0.09	0.02	Bal

5.1.1. Experimental steps

For each type of alloy, an ingot with approximately 30lbs was placed in a clay bonded graphite crucible, followed by heating up to 750°C in an induction furnace (Figure 5.1). After holding for 10 mins, a potato with 200 grams of weight was inserted into the molten metal to improve the initial hydrogen content in the melt so as to reflect the cleanliness ability of inert gas degassing. The moisture within the potato was decomposed to oxygen and hydrogen and entered the liquid. Once the potato was dehydrated for 20 min, it was taken out and the melt temperature was stabilized at 750°C. The probe of Foseco Alspek H system (Figure 5.2) was inserted into the melt to monitor the variation of hydrogen concentration during degassing. In the top of the probe, a calcium zirconate thimble coated with the reference material is installed as the sensor. When the probe was in the melt, different partial pressure of hydrogen generated voltage in the sensor that allowed the system to calculate the hydrogen concentration. The variation of hydrogen content with degassing time can be on-line displayed on the screen during the whole degassing process. Before degassing, two samples for RPT and density test were collected.

A rotary degasser (Figure 5.3) with a rotation rate of 110 rpm was used for degassing, and the set

flow value of argon gas was 2.5L/min. During degassing operation, the sample for density test was collected every 5 min, whereas the sample for RPT was collected every 10 min. The total degassing time is 45 min.



Figure 5.1. Picture of the induction furnace equipped with a graphite crucible



Figure.5.2. Foseco Alseck H system



Figure 5.3. Left: Photo of the rotary degasser; Right: Photo of degassing operation

The hydrogen level of the melt can be qualitatively by a Reduced Pressure Test (RPT). The melt was firstly ladled out to a small steel crucible followed by putting into a chamber, and then was vacuumed by the mechanical pump (Figure 5.4). Since the melt solidified in a low pressure environment, the pores in the melt would expand and become more evident than those formed under normal pressure. A RPT sample (Figure 5.4) was collected every 10 minutes and solidified under vacuum pressure for 15 minutes. To get the porosity distribution of the sample, each sample was analyzed by a VJ Technologies CT scanner ValueCT (Figure 5.5). The data was post treated using ImageJ (v1.52a) and three-dimensional images are created using the 3D viewer plugin. A sample was put on a rotatable platform in the machine. The X-ray was projected toward the rotating sample so that the cross-sectional (slide) of the sample from different angles can be obtained. An example of the CT scan results exported are shown in Figure 5.6. Each CT scan map consists of all of the CT scan slides of the sample, and the distribution of porosity can be obtained from top to bottom. With the post treatment by using Image J, the porosity within the sample can be extracted with a 3D representation.



Figure 5.4. Left: The picture of RPT machine; Right: The picture of a RPT sample



Figure 5.5. The picture of CT scan machine

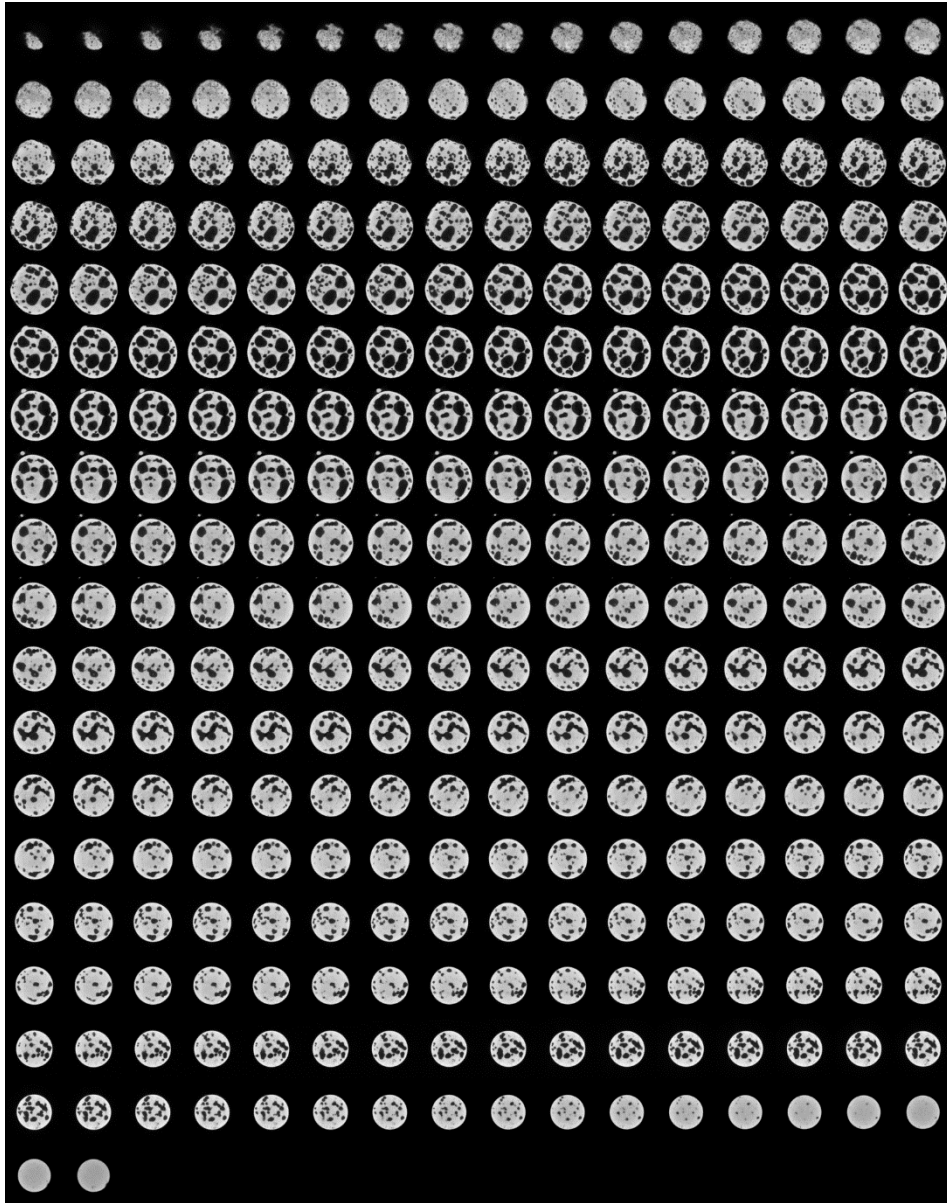


Figure 5.6. Montage of all of the CT scan slices of one of the RPT samples

It is well known that the density is greatly influenced by the content of porosity in the sample. More hydrogen content yields a lower density. Hence, besides the RPT sample, a small amount of melt was poured into a brass mold to obtain a density sample during degassing every five minutes (Figure 5.7). To get the precise result, the density was measured by Archimedes method in an electronic balance with density application attachment, in which the weight of a sample immersed in the water decreases the equal amount of weight of the water that the volume is equal to the sample (Figure 5.7). Thus, the density can be determined only by measuring the weight with 4 significant digits.

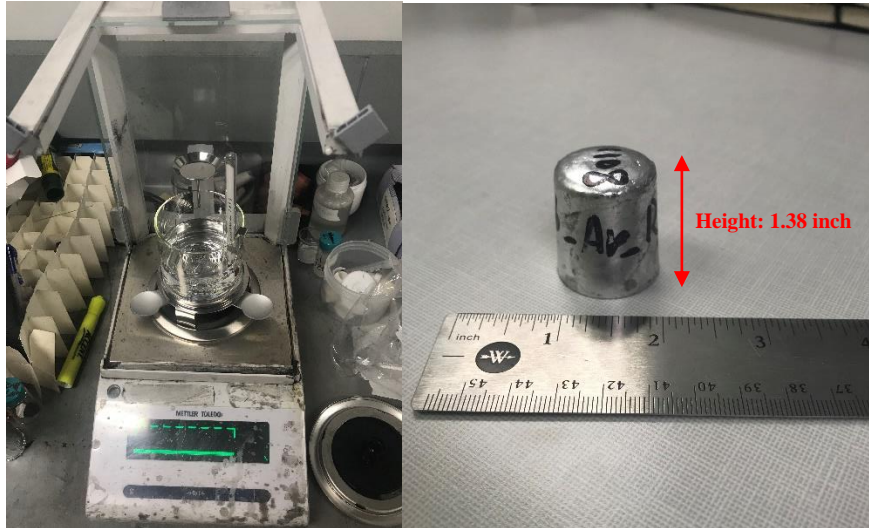


Figure 5.7. Left: The picture of electronic balance equipped with the density application attachments;
Right: A picture of a density sample

5.2. Metal-Mold Reaction

As learnt from the previous work, metal-mold reaction is regarded as another reason for the formation of defects. This section aims to prove this hypothesis by analyzing defects which were replicated under different conditions. Alloy type, cleaning procedure and mold type were selected as independent variables during casting. To make sure encompassing all variables and the efficiency of experiments, besides the experiments in WPI laboratory, another part of experiments were carried out in Palmer Foundry. Two kinds of aluminum alloy, A356 and C355 were used in the two trials. (Table 5.2)

Table 5.2. Composition of the aluminum alloys used (wt. %)

Alloy	Si	Cu	Mg	Fe	Ti	Al
A356	6.5	0.2	0.35	0.2	0.2	Bal
C355	4.5	1.5	0.5	0.2	0.3	Bal

5.2.1. WPI Trial

The designed experiments in WPI were used to compare the internal defects of different alloys purified by different cleaning procedures. Both A356 and C355 molten alloys were cleaned by Ar degassing without and with flux. For the comparison convenience, one trial without cleaning procedure was also made as the reference for each alloy. Besides, the RPT sample and chemical sample were cast for porosity and composition test, the mechanical properties were determined by

the tensile test. The microstructure and fracture morphology were characterized by optical microscope and scanning electron microscope (SEM).

5.2.1.1. Experimental procedures

Two types of aluminum alloys, A356 and C355, were melted. Three different trials without any cleaning procedures and with cleaning procedures (Ar degassing without flux, Ar degassing with flux) were applied to the same alloy. For convenience, they are designed as Reference trial, Ar trial and Flux trial, respectively. The weight of the ingot used in each trial is approximate 34-35 lbs. After melting, the molten alloy was poured into no-bake sand molds and ASTM standard (A823-99) steel molds. There were 18 sand molds from Palmer foundry, i.e. three samples from sand molds for each trial and three samples from steel mold.

Reference trial: The ingot was placed in a painted clay-graphite crucible and melted in the induction furnace, the molten aluminum alloy was kept at a temperature of $750\text{ }^{\circ}\text{C} \pm 5\text{ }^{\circ}\text{C}$ for 10 min. After removing the slags from the melt surface, two samples for chemical composition analysis and RPT were prepared. The molten aluminum alloy was first poured into three no-bake sand molds by a preheated ladle. The pouring weight for each sand mold was 7 lbs. Besides, four samples with around 3 lbs were collected by the ASTM steel molds (A823-99). The sand mold and the casting are shown in Figure 5.8. The steel mold and the sample are shown in Figure 5.9 (left) and Figure 5.9 (right), respectively. Before removing from the molds, the sand mold castings and steel mold castings were cooled in the molds for 45 min and 5 min respectively.

Ar trial: The procedure is similar to that for the preparation of the reference samples with the exception of the following process. After collecting the chemical and RPT sample, the preheated rotary degasser was inserted. To guarantee a constant cleaning procedure, a graphite baffle was inserted into the melt. The rotary degasser and the baffle can be seen in Figure 5.10 (left) and Figure 5.10 (middle), respectively. The flow of argon was 2.5L/min and the rotary rate was 500 rpm. After degassing for 20 min, the RPT sample and three samples from sand molds and four samples from steel molds were collected.

Flux trial: The procedure is almost the same as the Ar samples except for the following differences. At the melt temperature of $750\text{ }^{\circ}\text{C}$, the preheated rotary degasser was inserted followed by rotating till the formation of a vortex. 20g of flux granules were poured into the vortex and stirred for 0.5

min till all the granules dissolve into the melt. The flux composition is listed in Table 5.3. A graphite baffle was inserted into the melt to suppress the vortex formation so that the flux can be mixed with the melt properly without introducing more oxides. The flux insertion system is shown in Figure 5.10 (right). After degassing for 20 minutes, the surface slags were skimmed and the same procedure was repeated similar to Ar and reference trial.

Table 5.3. The composition of the flux (COVERAL GR 2531)

Composition	Content (wt. %)
KNO ₃	3-7
Na ₂ CO ₃	3-7
NaCl	60-80
Na ₂ SO ₄	10-20
CaF ₂	5-10

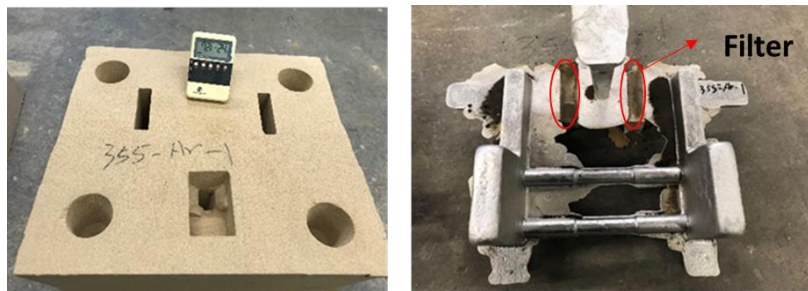


Figure 5.8. Left: Picture of sand molds from Palmer Foundry. Right: The casting by the sand mold



Figure 5.9. Left: Picture of ASTM standard steel mold. Right: The casting from the steel mold



Figure 5.10. Left: The design of the degassing impeller. Middle: The picture of graphite baffle. Right: View of the flux insertion system

5.2.1.2. Tensile test

Internal defects deteriorate the mechanical properties of castings. Therefore, it is necessary to evaluate the relation of the different level of defects and the tensile strength of castings under different conditions. In WPI trial, both samples from sand molds and steel molds were cast as tensile bars. The tensile bars from sand molds and steel molds are shown in Figure 5.11. The tensile bars from sand molds were cast to the ASTM B557 standard size, whereas the tensile bars from steel mold were followed with ASTM A823.

The tensile test were performed in an Instron Load frames (Series 5500R). During tensile test, an extensometer was clamped on the bar to get more precise strain value with four significant digits. A snap of test process and the extensometer are shown in Figure 5.12.

The gage part of all the ASTM standard steel molds has a diameter of 0.5 inch and the gage diameter with 0.63 to 0.65 inch for bars from the sand molds. All stress and strain were recorded by the Bluehill 3. In the software, the diameter of sand mold tensile bars from the same trial are set as a constant number which is the average diameter of the trial. However, after the test, all the tensile strength was recalculated with the real gage diameter and the stress-strain curves were drawn by the Microsoft Excel.



Figure 5.11. Left: Tensile bars from sand molds (one trial). Right: Tensile bars from steel molds (one trial)



Figure 5.12. Left: Tensile test. Right: extensometer

5.2.1.3. Fracture surface

By comparing the mechanical properties of tensile bars with different independent variables, it can better understand the dependence of these variables with the different level of defects. Additionally, to get the deep insights of those defects, the fracture morphologies and chemical composition were characterized by a stereo optical microscope (Nikon SMZ 1500) and the JEOL JSM-7000F scanning electron microscope (SEM) equipped with the Oxford Instruments energy dispersive spectroscopy (EDS) detector.



Figure 5.13. Nikon SMZ 1500 stereo optical microscope

5.2.2. Palmer Trials

Besides the internal defects that were analyzed in WPI trials, the Palmer trial aims to figure out the effect of metal-mold reaction on the surface defects. Two types of sand mold, green sand and no-bake sand were provided by Palmer Foundry. Also, argon degassing and mixed gaseous chlorine with argon degassing were applied on the molten A356 and C355 alloy in the Palmer Foundry.

It is noted that the spiral pattern molds for the fluidity test were provided by Palmer Foundry, as well as the molds with radius pattern, which is a cuboid with the same curve sag on both sides of the long side, so as to analyze the reaction occurred on the casting surface.

All the melting, cleaning and pouring were conducted in the Palmer Foundry. Figure 5.14 shows the melt ladles used in the trials. The melt temperature was 720°C, the set gas pressure for both argon and chlorine was 32 ± 5 psi and the flow rates were 20 ± 3 SCFM (standard cubic foot per minute) for argon and 3 ± 0.5 SCFM for chlorine, and the degassing time was 20 minutes. Totally 6 samples from spiral molds and 16 samples from radius molds were prepared in the Palmer Foundry, and the detail are given in Table 5.4.



Figure 5.14. The picture of ladles used in Palmer Foundry

Table 5.4. Samples from Palmer Trials; (a) samples for fluidity test; (b) samples for surface roughness analysis

(a)	
C355	A356
No-bake sand reference	No-bake sand reference
No-bake sand with argon	No-bake sand with argon and chlorine
No-bake sand with argon and chlorine	\

(b)	
C355	A356
No-bake sand reference	No-bake sand reference
No-bake sand with argon	No-bake sand with argon
No-bake sand with argon and chlorine	No-bake sand with argon and chlorine
Green sand reference	Green sand reference
Green sand with argon	Green sand with argon
Green sand with argon and chlorine	Green sand with argon and chlorine

5.2.2.1. Fluidity

Besides above mentioned four hypotheses, another possible reason for the formation of defects is that cleaning procedures could influence the fluidity of the melt. It is more difficult for the melt with poorer fluidity to fill the cavity in the mold. Therefore, to reveal the effect of cleaning procedures on the melt fluidity, the fluidity test was made.

The length of spiral equals to the distance that melt flow till its full solidification, which can represent the fluidity of molten metal. The flow length of six spiral test samples were measured by the same cotton thread. A spiral sample for the fluidity test is shown in Figure 5.15. Two measurements were made for each sample and the thread was pulled from the start point to the spiral tip in each measurement.



Figure 5.15. A spiral sample for fluidity test

5.2.2.2. Surface roughness

The metal-mold reaction may happen at the interface between melt and mold, which results in the formation of defects on the casting surface. Figure 5.16 shows the sample obtained from radius mold for the analysis of metal-mold reaction. The curve section on both sides of the sample aims to increase the area of the interaction. If the reaction happens at the interface, it perhaps causes an uneven surface. Hence, it is necessary to measure surface roughness for better understanding of the formation of the different level of defects.

Generally, the most universally used parameter for surface roughness is the arithmetic height average (Ra), which is defined as the average absolute deviation of the irregularity from the mean line over one sampling length (Figure 5.17) ^[13]. The mathematical definition and digital definition are given as follows.

$$\text{Mathematical definition of Ra}^{[13]}: Ra = \frac{1}{l} \int_0^l |y(x)| dx \quad (5.1)$$

$$\text{Digital definition of Ra}^{[13]}: Ra = \frac{1}{n} \sum_{i=1}^n |y_i| \quad (5.2)$$

The curve section was cut from the casting sample for the CT scanning (Figure 5.16). To obtain the surface profile, the CT scan images of each sample were imported into the VGSTUDIO MAX (V3.1) to construct the 3D representation (Figure 5.18). Since the 3D construction is composed of all images of the sample and each image represents a plane of the sample, by moving the clipping plane on the 3D object, the plane of the sample can be selected, and the contour of the object can be regarded as the surface profile (Figure 5.18). In the following analysis, 10 planes for each sample were extracted to obtain contours (4 planes from the thick section, 4 planes from the thin section and 2 planes from the arc section).

The image that was obtained from VGSTUDIO MAX was imported in MATLAB and transferred

to a grayscale intensity image from a true color image. Each image consisted of numbers of pixels in MATLAB after transformation as shown in Figure 5.19. Unlike the true color image, in which each pixel is represented by three values (RGB), for the grayscale image, only one value is contained in each pixel and represents the brightness of each pixel. Furthermore, using grayscale intensity instead of RGB, which can be seen as a vector that contains three numbers, can simplify the analysis. Since there were no other colors in the image except black and gray colors, no information of image was missing during the transformation. The larger pixel value represents the point of the sample at which the density is higher. Likewise, the lower density point is represented by the smaller pixel value. When a pixel value is less than a threshold, it can be regarded as no object at this point.

To simplify the calculation, each image was cropped in ImageJ (V 1.52a), and only the section near the boundary that needs to be analyzed was left. A series of script in MATLAB was used to collect the position of the pixel whose value was first above the threshold in each column. The threshold value was 55 for all samples. It is worthy to note that the same pixel value in different samples does not represent the same density, it is just a relative value. Once the pixel value in all samples was lower than 55, clear objects do not exist. So, the threshold value was selected as this number.

The surface profile was extracted by combining positions of those collected pixels. The extraction result are shown in Figure 5.20. Then the polynomial curve for the profile can be fitted by MATLAB. This polynomial curve was regarded as the mean line to calculate the Ra. Hence, the calculation of Ra is written as follows:

$$Ra = \left[\frac{1}{n} \sum_{i=1}^n |y_i| \right] * m \quad (5.3)$$

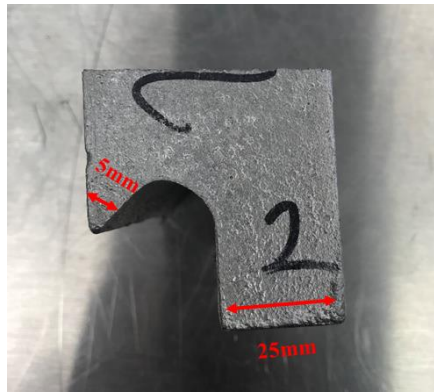
where m is the height of each pixel and $|y_i|$ is the distance between the profile line and the mean line and n is the number of pixels that collected. The actual height of each pixel was 0.112mm at the magnification that was applied during analysis.

To verify the accuracy of this measurement method, a polished sample with the smooth surface was scanned and measured in MATLAB with the same script. The result can be seen in Figure 5.21. A perfect straight line was obtained and the roughness was zero.



(a)

(b)



(c)

Figure 5.16. (a) Casting sample from the radius mold (b) curve section from the sample
(c) Thickness of the sample

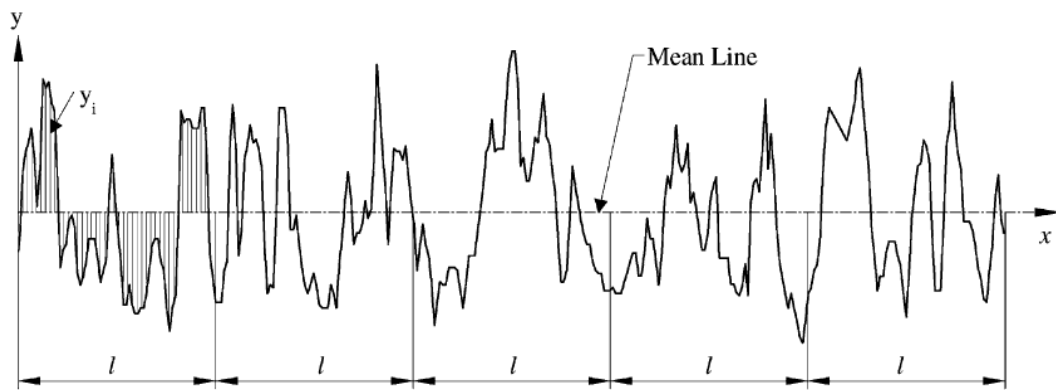


Figure 5.17. Definition of Ra ^[48]

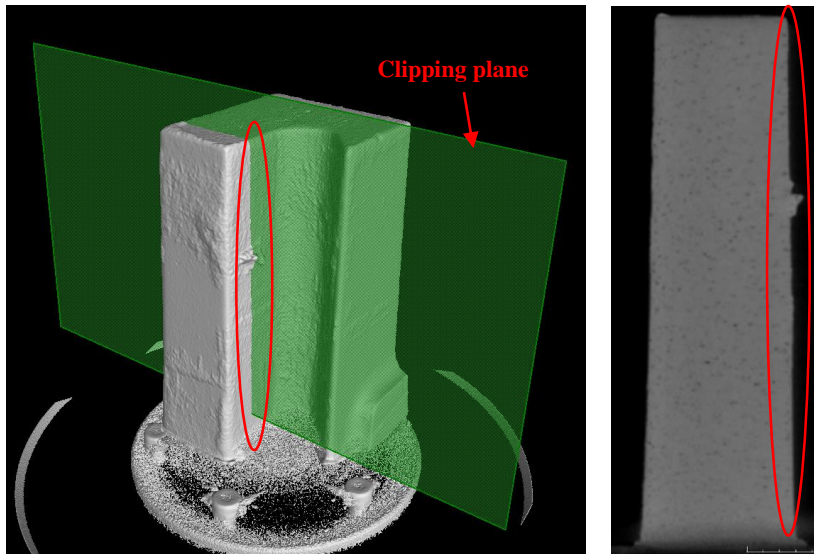


Figure 5.18. Extraction of the surface profile. Right: 3D construction of a sample; Left: A selected plane of the sample

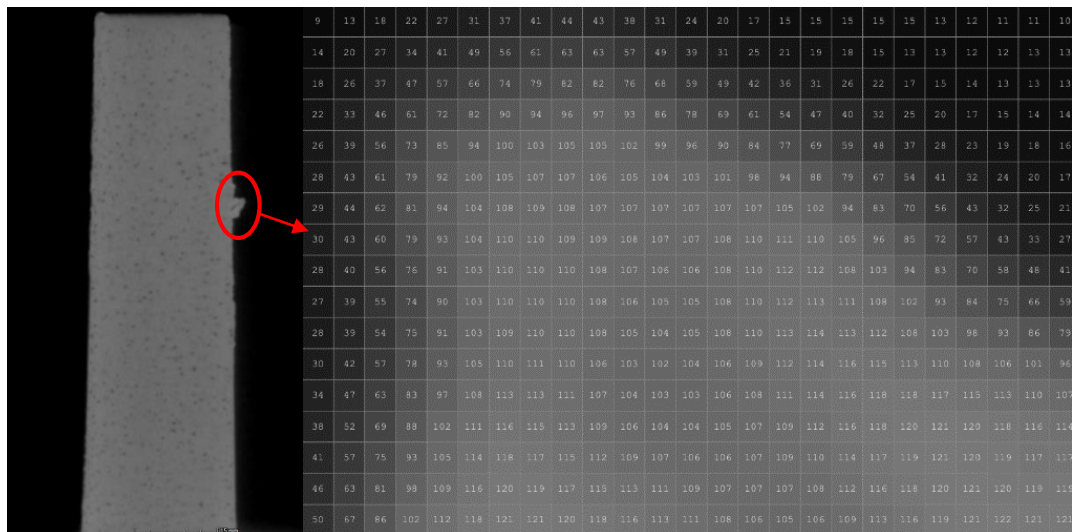


Figure 5.19. Pixel value of the object.

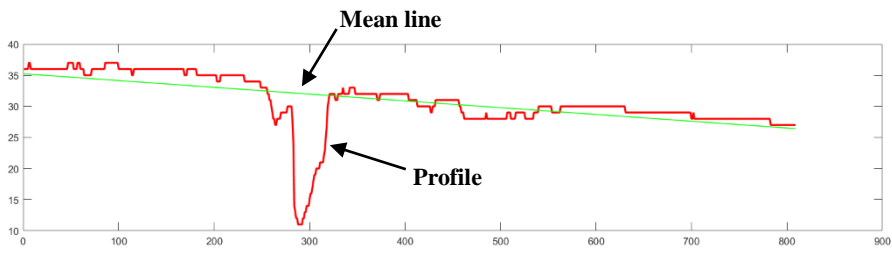


Figure 5.20. Matlab result of one surface

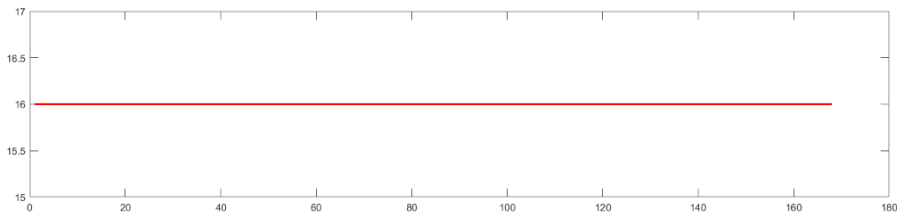


Figure.5.21. Verification of Matlab method

6. Results and discussion

6.1. Effectiveness of hydrogen extraction

6.1.1. Hydrogen content

Figure 6.1 and Figure 6.2 show the Alspek results of A356 and C206 aluminum alloys, respectively. The results show that hydrogen content significantly decreases with degassing time. The hydrogen content decreases sharply at the early stage while it decreases slightly with increasing degassing time. Additionally, it is evident that the curve of hydrogen content is not smooth. This is most likely due to its sensitivity to the change of temperature. It is true that the solubility of hydrogen is closely related to the melt temperature, and the variation of temperature may affect the change of hydrogen content. However, in this case, it is worthy to note that the unsmoothness of the curve of hydrogen content is also related to the principle of the measurement. The result of hydrogen content that is obtained from Alspek H system is calculated by the partial pressure of hydrogen in the melt. The instability of temperature that is caused by the induction furnace would influence the hydrogen partial pressure and therefore influence the result of hydrogen content and unsmooth curves. Both two hydrogen content curves show that the hydrogen content decreases sharply at the initial stage while the decreasing rate reduces afterwards. During rotary degassing, purged gas bubbles are inserted into the melt. Since the concentration gradient of hydrogen exists around bubbles, the atomic hydrogen that dissolve in the melt form the molecular hydrogen and pass through the interface of gas and melt to enter the bubbles. Hence, the hydrogen can be extracted and taken to the melt surface with the inert gas bubbles. At the early stage, the hydrogen content is higher, more atomic hydrogen exists in the melt, which means it is easy for inert gas bubbles to catch hydrogen. Nevertheless, this process gets harder when there is less hydrogen in the melt. Therefore, the hydrogen content decreases sharply at the beginning of the degassing and it is more difficult to extract the hydrogen with degassing time goes on.

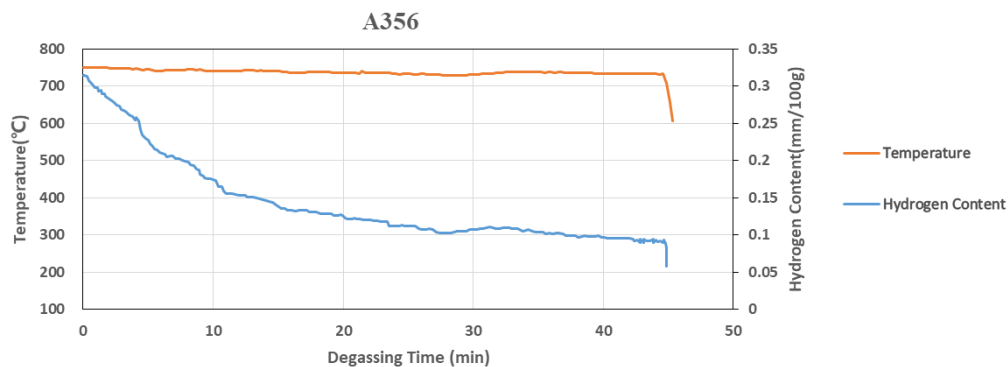


Figure 6.1. Alspek H measurements of temperature and hydrogen content during degassing of A356

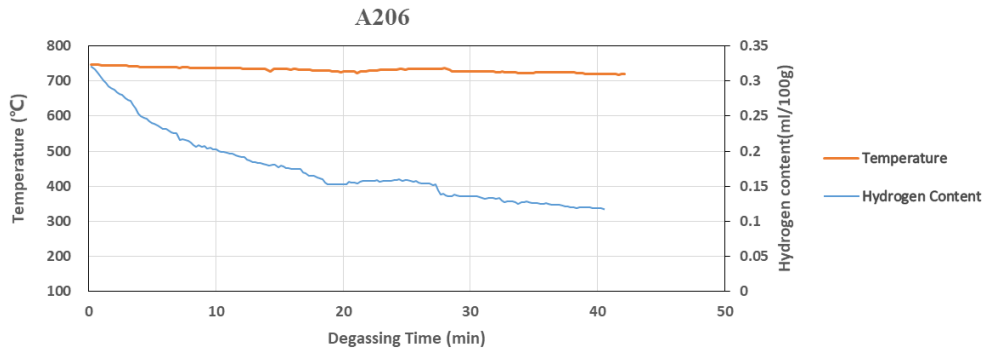
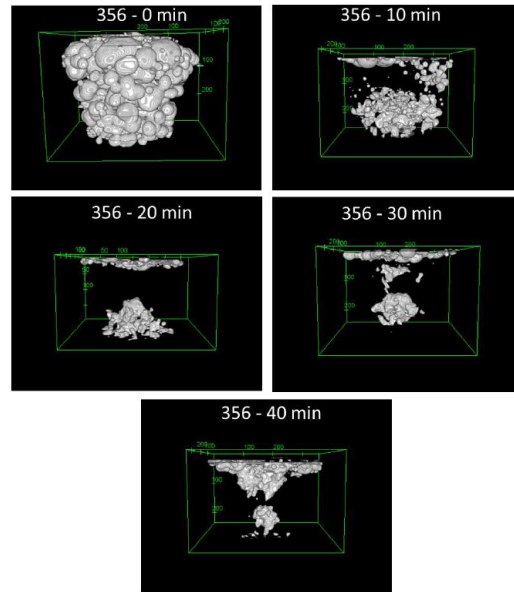


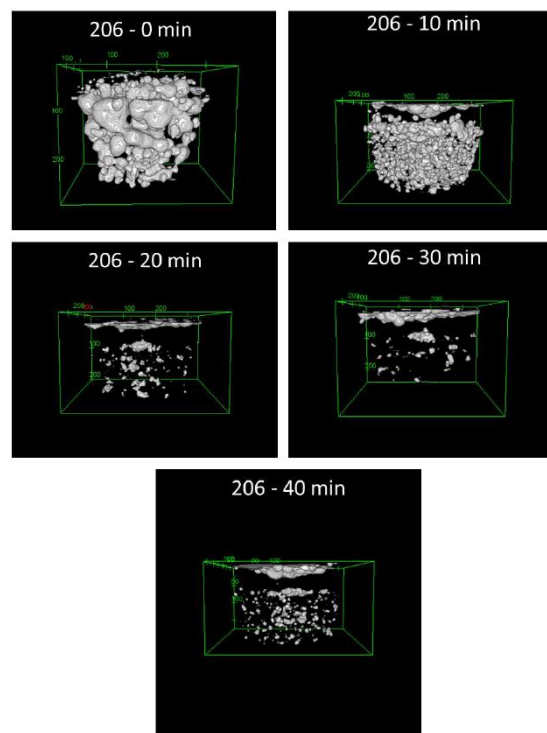
Figure 6.2. Alspek H measurements of temperature and hydrogen content during degassing of A206

6.1.2. Porosity distribution

The distribution of the porosity existed in the reduced pressure test samples with different degassing time for A356 and A206 aluminum alloys are shown in Figure 6.3. Similar to the measured results of hydrogen content measurements that are shown above, the amount of porosity in both samples decreases obviously from the beginning to 20 min. Whereas its reduction trend is not significant after degassing for 20 min. Granted, it is hard to directly distinguish the origin of porosity by using the CT scan. Consider the location and the shape of the porosity that leave in the melt after 20 min of degassing, the origin of these residual porosity seems to be different for A356 and A206 aluminum alloys. For A356 aluminum alloys, most of the porosity seems to be shrinkage porosity are located at the center of the sample. However, for A206 aluminum alloy, the amount of porosity has no significant decrease after degassing for 20 min, though the porosity distributes more evenly. Most of the porosity present has a round shape, which may indicate they are originated from the hydrogen. In addition, the influence of copper content in the alloy may cause this difference. Indeed, these evenly spread porosity in A206 may refer to the hydrogen microporosity. It is agreed that microporosity is easier to form in Al-Cu alloy than Al-Si alloy, which can be explained by their phase diagrams (see Figure 6.4 ^[10]). It can be seen that Al-Cu alloy has wider mushy zone than Al-Si alloy, which can increase the formation of the microporosity ^[11]. Additionally, in Al-Si system, with the addition of copper element, more porosity can be found. Caceres, C. H., et al ^[12] found that, when the Cu content is over 0.2% in Al-Si-Mg alloy with Sr modification, the dispersed microporosity increases seven times. Figure 6.5 ^[11] also shows the relationship between the volume fraction of porosity and the copper content in the alloy.



(a)



(b)

Figure 6.3. Porosity distribution of reduced pressure test samples with different degassing time

(a) A356; (b) A206

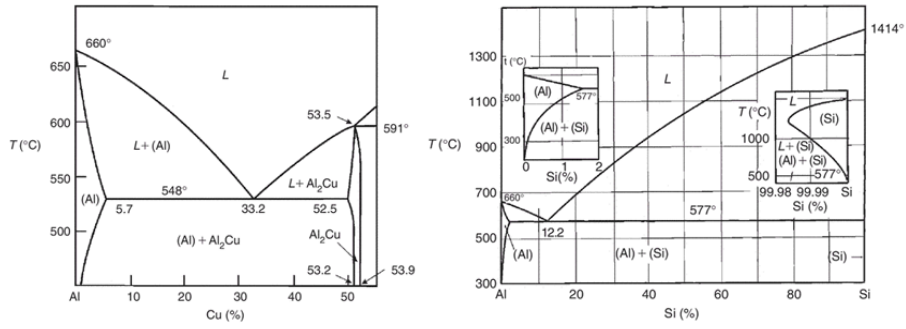


Figure 6.4. Phase diagrams of Al-Cu and Al-Si [10]

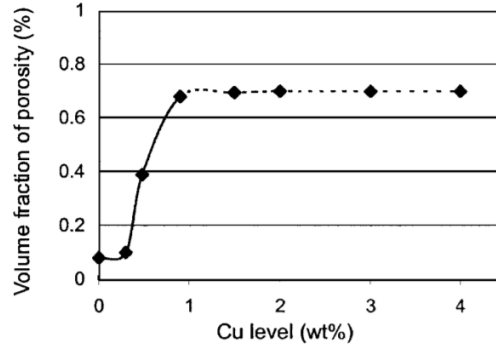
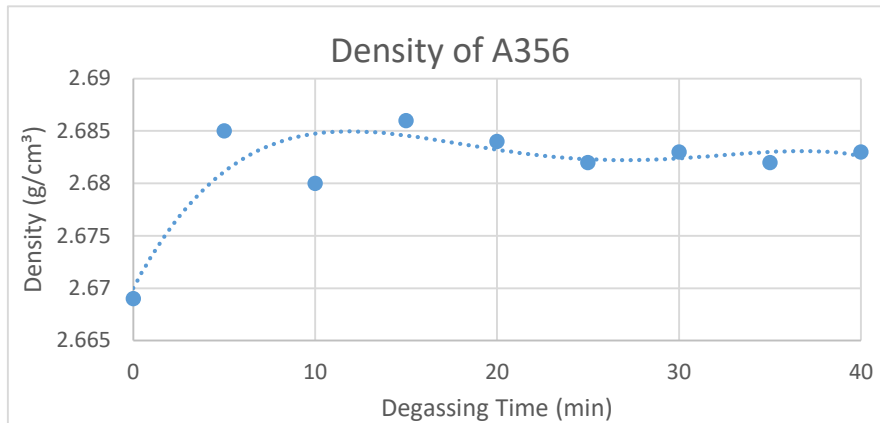


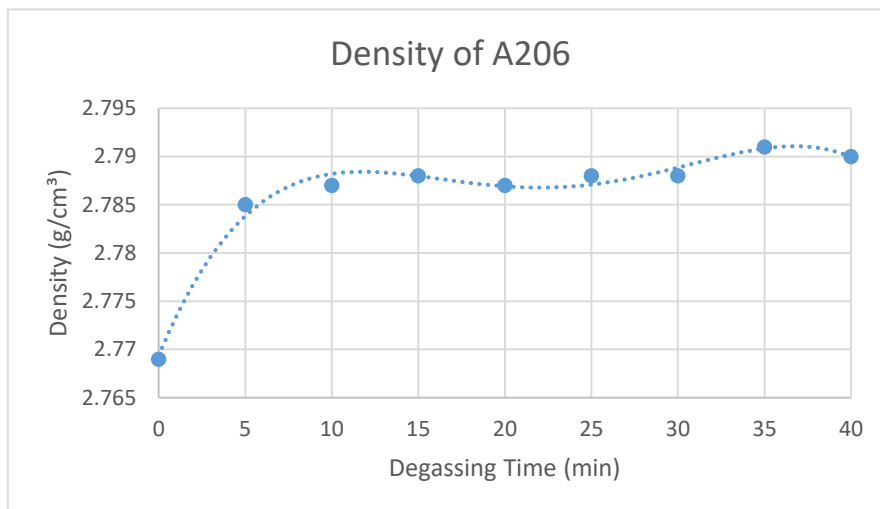
Figure 6.5. The effects of Cu content on porosity fraction in Al-Si alloy [9]

6.1.3. Density measurement

Figure 6.6 shows the variation of density with degassing time. Generally, the density of samples for both alloys increases with increase of degassing time as the hydrogen content decreases. At the initial stage, the density increases significantly, which is in good accordance with the change of hydrogen content shown above. The reduction rate of hydrogen concentration is larger at the beginning of the degassing than the later stage.



(a)



(b)

Figure 6.6. The measured density of A356 (a) and A206 (b) at different degassing time

6.2. Internal defects

6.2.1. Chemical composition

The chemical compositions for the samples with different cleaning procedures were analyzed by the optical emission spectroscopy (OES) and were compared with the standard alloy. The results are given in Table 6.1, in which R, Ar and Fl represent reference trial, Ar degassing trial and flux trial, respectively. For comparison, the chemical compositions of standard alloys (from ASM alloy database) are also listed in the Table 6.1.

Specially, the composition of calcium and sodium were analyzed to determine whether the addition of flux granules influences the composition of the melt by introducing extra substances. As learnt from the results of samples with different cleaning procedures, only tiny calcium and sodium exist, indicating that the addition of flux granules did not affect the final composition of the melt. In fact, the flux tablets can prevent from forming oxides in the aluminum melt based on the thermodynamic theory. The sodium and calcium prefer form chlorides and fluorides and float on the melt surface which are removed before pouring.

Compared the chemical compositions among different trails, it is found that no significant change occurs for these elements. Besides, their contents are all in the range of standard alloy though they are treated by different cleaning procedures. Subsequently, it is thought that the substances used during cleaning have no influence on the melt.

Table 6.1. Chemical composition of samples with different cleaning procedures (wt. %)

Sample	Si	Cu	Fe	Mg	Ca	Na	Al
C355-R	5.34±0.075	1.35±0.025	0.121±0.0048	0.62±0.012	0.0013±0.0009	0.0002±0.0002	92.4±0.053
C355-Ar	5.37±0.041	1.36±0.0031	0.123±0.006	0.6±0.0014	0.0004±0.0003	0.0001±0.0001	92.4±0.064
C355-Fl	5.37±0.036	1.33±0.026	0.124±0.0067	0.61±0.011	0.0015±0.0011	0.0005±0.0001	92.4±0.059
C355	4.5~5.5	1~1.5	≤0.2	0.4~0.6	\	\	91.8~94.1
A356-R	6.68±0.064	0.0001±0.0003	0.097±0.0087	0.382±0.047	0.0014±0.0015	0.0003±0.0003	92.7±0.094
A356-Ar	6.55±0.078	0.0001±0.0002	0.085±0.0073	0.344±0.042	0.0015±0.001	0.0003±0.0003	92.9±0.115
A356-Fl	6.71±0.074	0.0001±0.0001	0.088±0.0083	0.306±0.007	0.0019±0.0023	0.0002±0.0003	92.7±0.0069
A356	6.5~7.5	≤0.2	≤0.2	0.25~0.45	\	\	91.3~93.2

6.2.2. Degassing effectiveness

To evaluate the effectiveness of different cleaning methods, an RPT sample was cast from each trial. It has been proved that hydrogen can be extracted by degassing with argon in the previous experiments. However, the cleaning ability between argon trial and flux trial is still unclear. The RPT sample used here is the same as that shown in Figure 5.4. Each sample was scanned by CT machine and the results are shown in Figure 6.7 and Figure 6.8. In the two figures, each column consists of images that were collected from one sample with four angles of rotation (0°, 90°, 180°, and 270°).

Similar to the results shown in figure 6.5, the amount of porosity in the sample reduced drastically after Ar degassing, and the porosity left after cleaning are most likely from shrinkage according to their shape and location. Compared to A356, there are more porosity in the sample of C355 with higher copper content before cleaning. In fact, based on Ye's work^[11], more porosity tend to form with the increase of copper content. Of course, the type of these porosity cannot be distinguished only by using CT scanning. It is worthy to indicate that most of the porosity present strip shape in C355 aluminum alloy which should be related to the oxide bifilms. Also, compared to the reference trial, the result shows obviously improvement after flux treatment. Though, it can be suggested that both of these two cleaning methods can avoid the influence from hydrogen, it is not clear that there are any significant differences between the results from the argon trial and the flux trial. Due to the floated dross on the melt surface, which could hinder the escape of the hydrogen, it seems that there are a little more defects in samples of flux trial than that of argon trial.

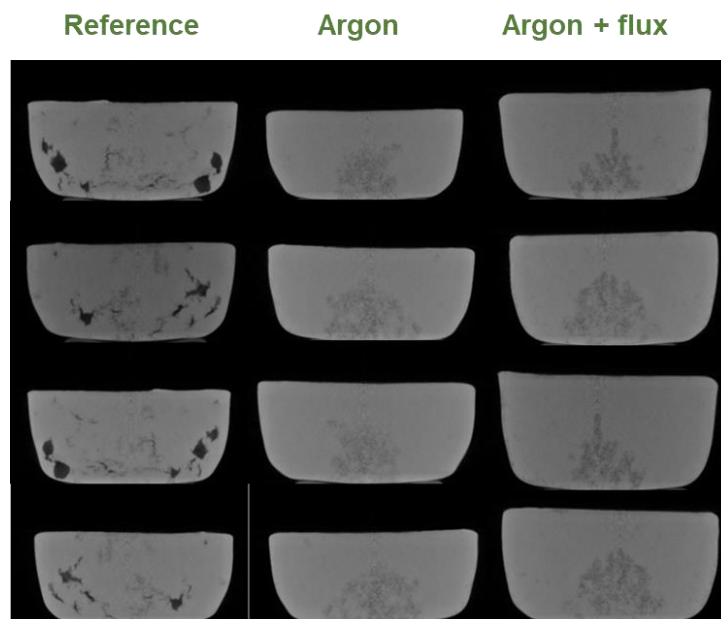


Figure 6.7. CT scan results of RPT samples with different cleaning procedures (A356)

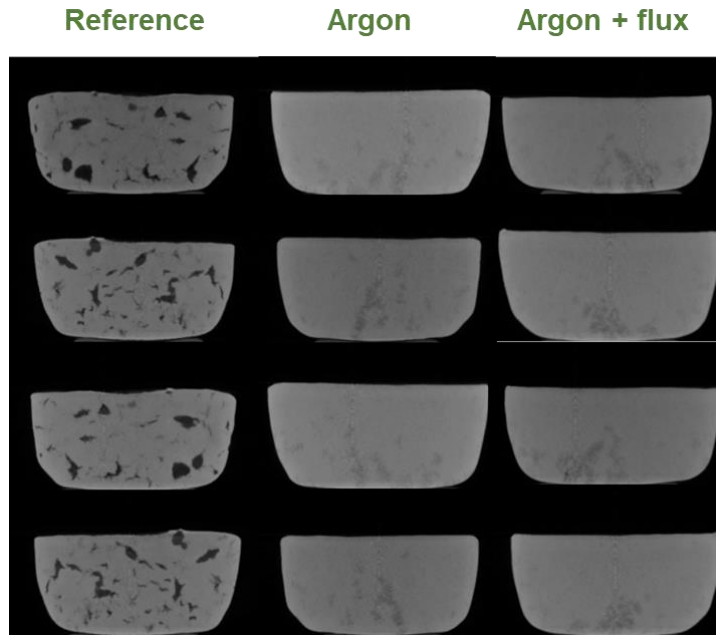


Figure 6.8. CT scan results of RPT samples with different cleaning procedures (C355)

6.2.3. Mechanical properties

The change of mechanical properties can be regarded as an indirect way to disclose the effect of different parameters on internal defects. By comparing the mechanical property of samples with different casting parameters, it can determine whether the defects occur inside the sample and which is the dominated factor cause the formation of defects. Thus, the tensile tests were conducted, and the number of tensile bars from each trail are listed in Table 6.2. The “ref”, “Ar” and “Flux” represent reference trial, argon trial and flux trial, respectively. All tensile bars were scanned by the CT machine before the tensile test so as to verify if hydrogen porosity exists inside the sample.

All the tensile test data were collected and exported as the stress-strain curves which are shown in Figure 6.9 and Figure 6.10. Each graph consists of all stress-strain curves of tensile bars from the same trial. It can be seen that most of the curves contain hops for the samples from sand molds. The hop is derived from the slip between the tensile bar of the sand mold due to uneven surface, and the fixture on the load frame. Though these hops may slightly influence the accuracy of the data, the differences between each trial is so small. So it is believed that the results can be used to represent the tensile strength.

The average ultimate tensile strength and failure strain for each trial of A356 and C355 aluminum alloys are shown in Figure 6.11 and Figure 6.12, respectively. Generally, C355 has better strength and larger ductility than A356, which is as expected. The results from the tensile tests of A356

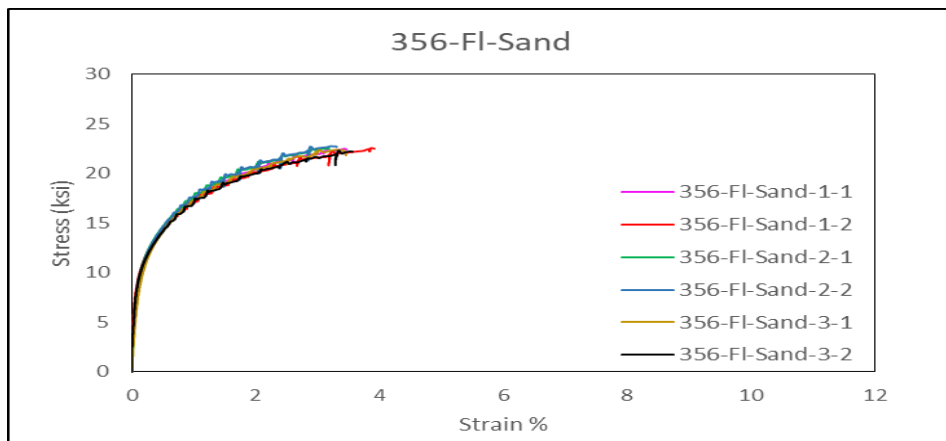
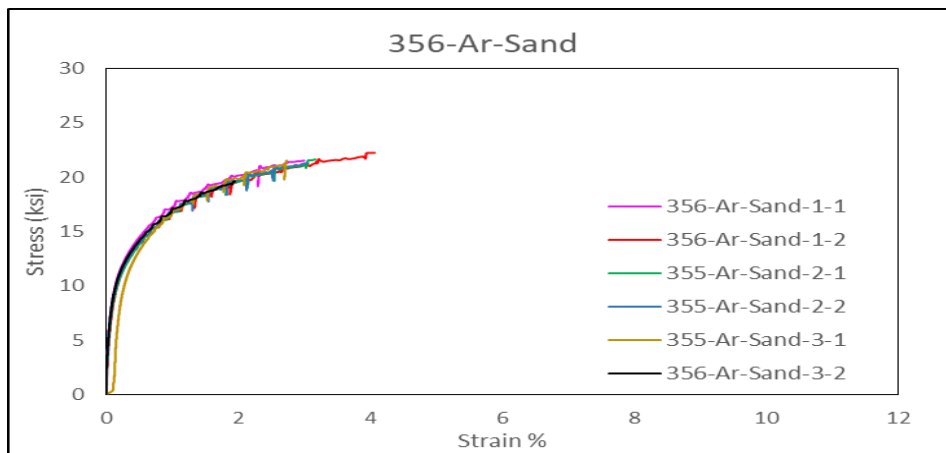
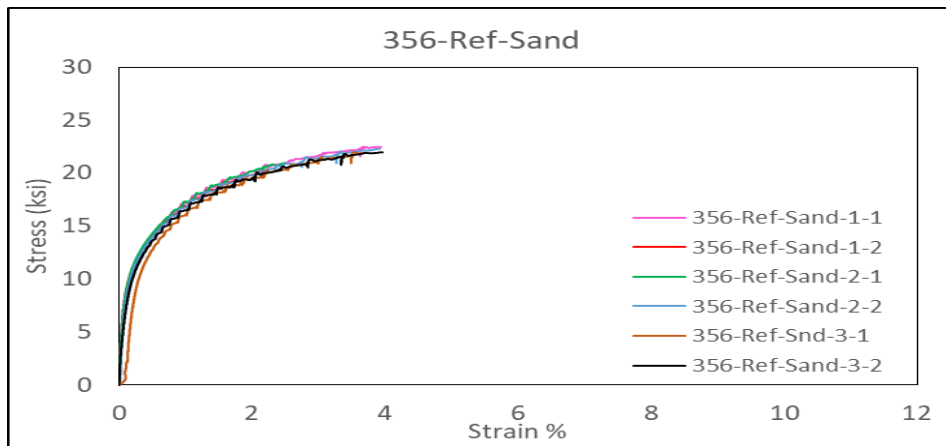
prepared by steel mold show that the ultimate tensile strength (UTS) improves a little (6% with argon degassing and 7.2% with flux cleaning) and elongation is increased by almost two times after flux cleaning. However, it can be seen from other three figures that there are no obvious improvements in other tensile tests. Compared to the reference trial, the UTS improves 6.7% at most in all flux trials. For argon trial, though, samples of C355 with sand mold represent relatively more improvement on UTS (10.2% with argon degassing), the UTS reduce on samples of C355 with steel molds and on samples of A356 with sand molds. In order to rule out the possibility of residual hydrogen porosity in the samples that could suppress the improvement on mechanical properties, tensile bars were scanned by the CT machine, the results are shown in Figure 6.13 and Figure 6.14. The results verify that the hydrogen porosity can be extracted by any one of the cleaning method. Hence, it is believed that there are other defects exist in the sample influence the mechanical properties.

On the one hand, the inclusions or oxides which were produced during the whole casting process left in the sample could be the main reason for the poor mechanical properties instead of the hydrogen. Thus, it is hard to improve the mechanical properties even though the hydrogen porosity was eliminated. On the other hand, besides the original defects that formed during process, new oxides generated during cleaning may deteriorate the quality of the sample. Oxides may be produced in two ways. First, during degassing process, the rotary degasser not only extracts the hydrogen, but the occurred turbulence promotes the formation of oxides bifilms in the melt with the entrapped air. Second reason is that the oxides may generate by the occurred turbulence in the mold which is possibly due to the improper gating system, which was proposed as one of the hypothesis in hypothesis section (Chapter 4).

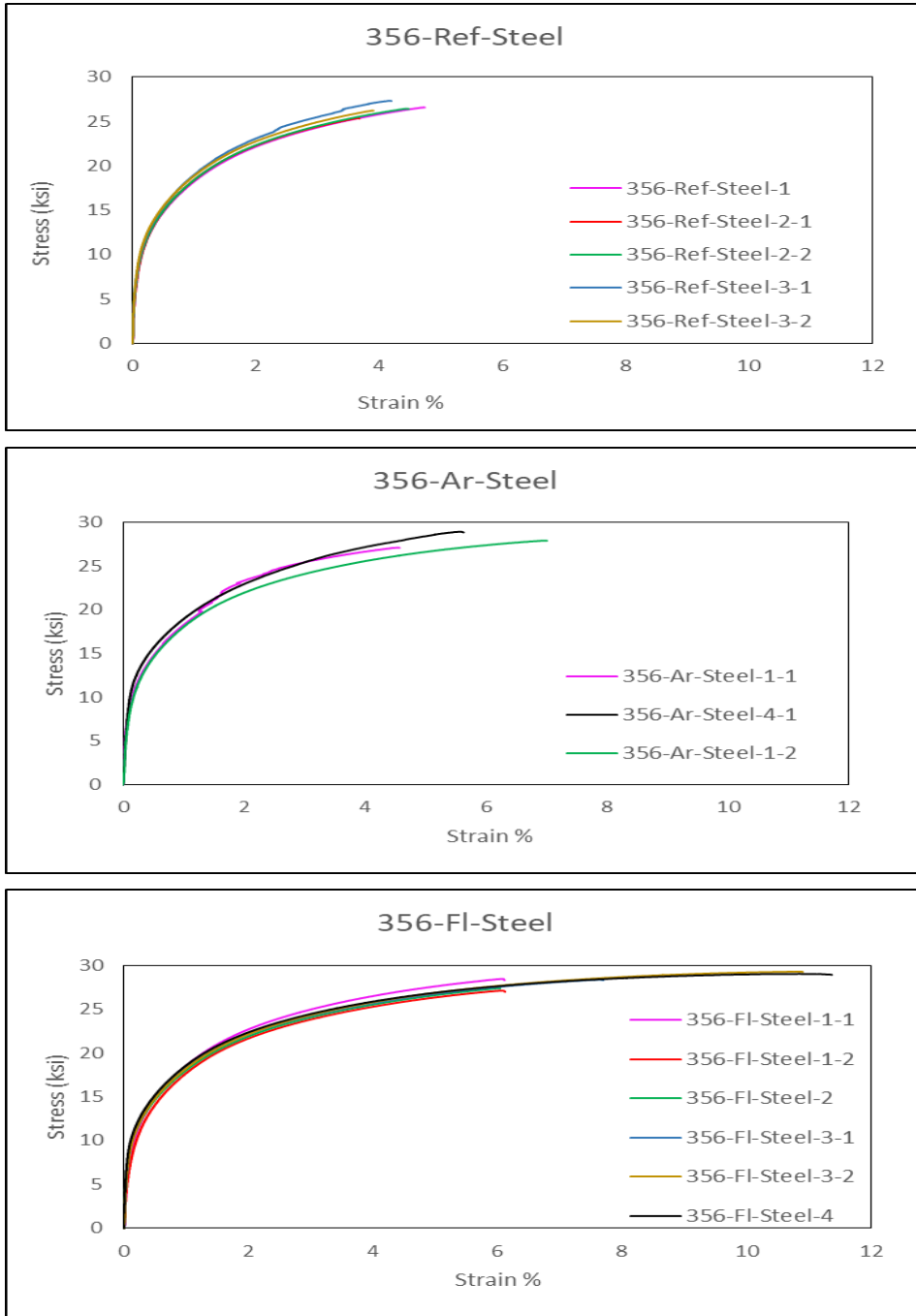
Based on the results for the same alloy with the same cleaning procedures, it is clear that the sample made from steel mold have better strength and larger elongation. It is caused by the difference of their cooling rate. The cooling rate is far larger in the steel mold than in the sand mold, which can contribute the finer microstructure and, thus, result in the better mechanical properties. This can be verified by the microstructures of samples from different types of molds, see Figure 6.15.

Table 6.2. The number of tensile bars from each trial

Trial	Number	Trial	Number
A356-Ref-Sand	6	A356-Ref-Steel	5
A356-Ar-Sand	6	A356-Ar-Steel	3
A356-FI-Sand	6	A356-FI-Steel	6
C355-Ref-Sand	6	C355-Ref-Steel	6
C355-Ar-Sand	6	C355-Ar-Steel	6
C355-FI-Sand	6	C355-FI-Steel	6

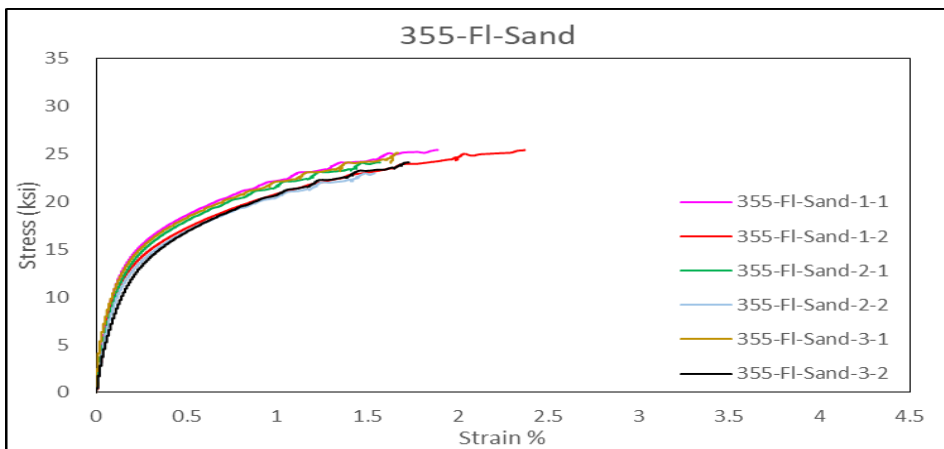
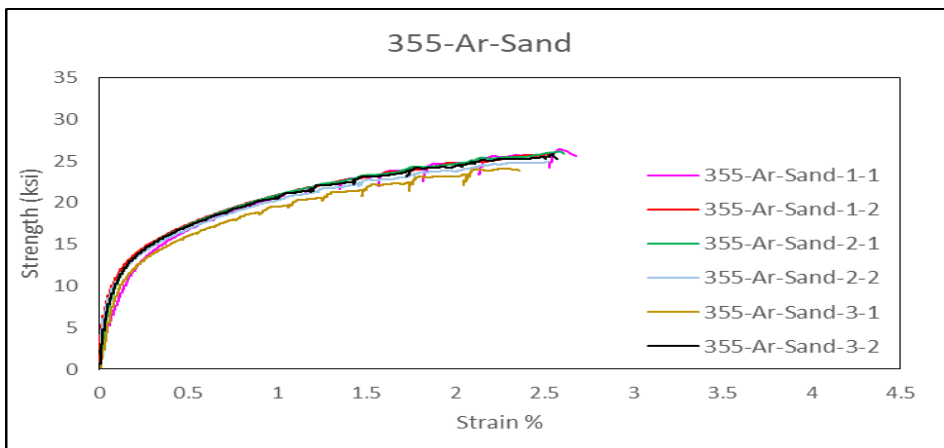
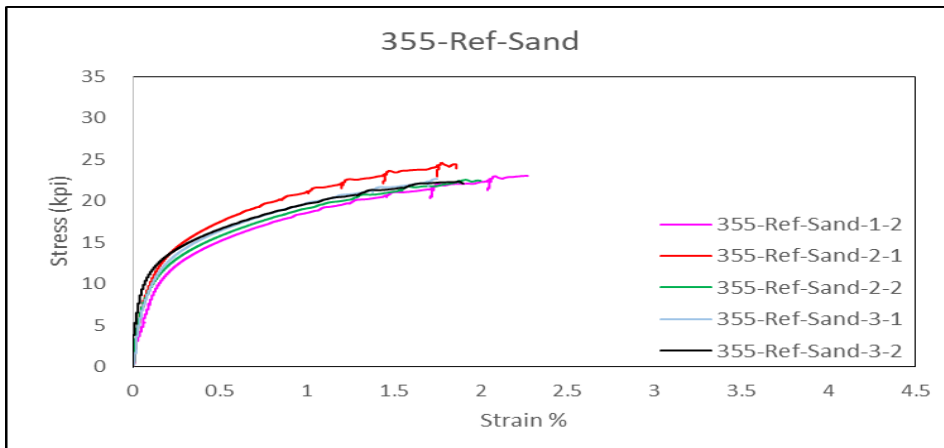


(a)

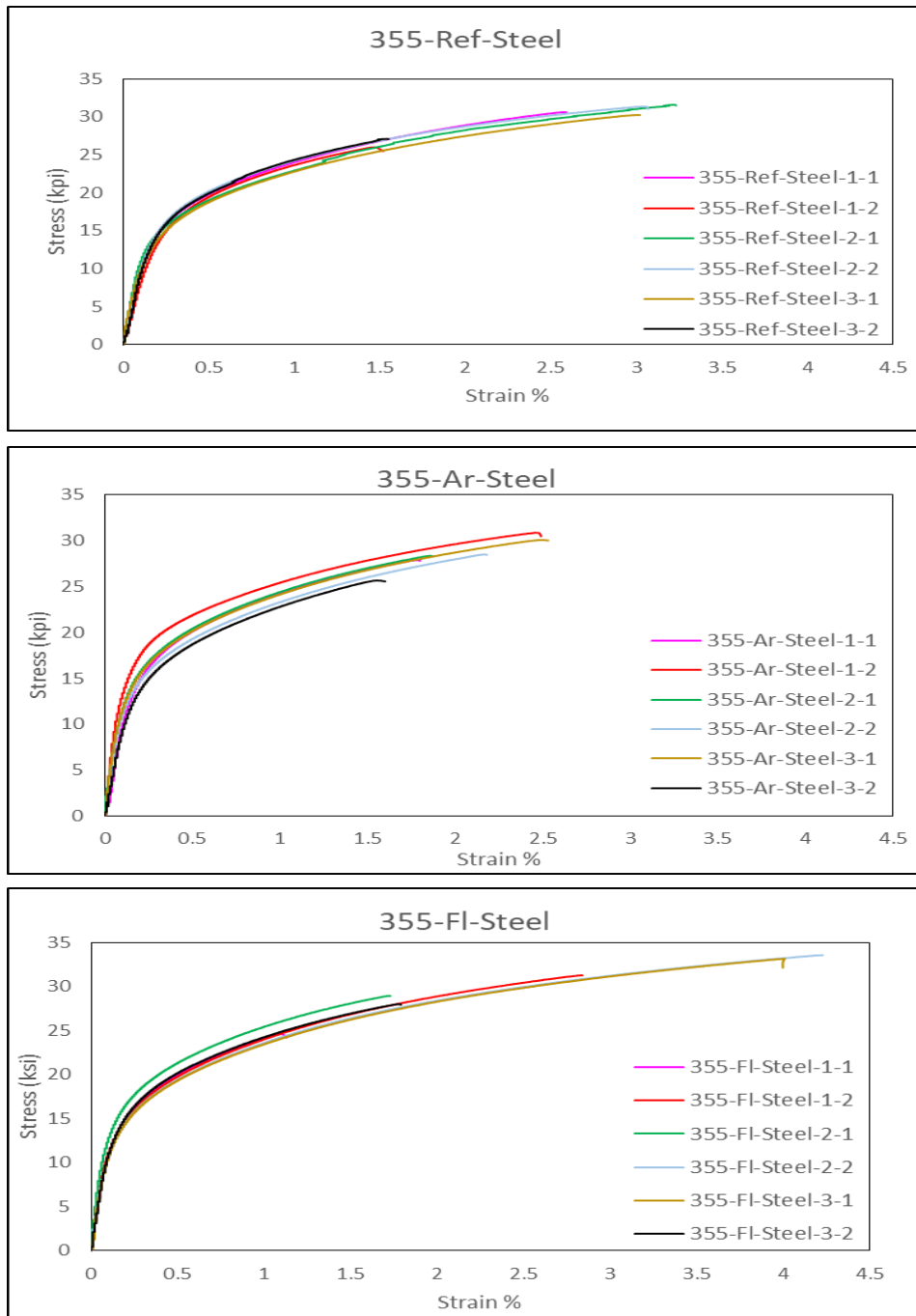


(b)

Figure 6.9. Stress-strain curves of A356 aluminum alloy under different conditions (a) sand mold (b) steel mold

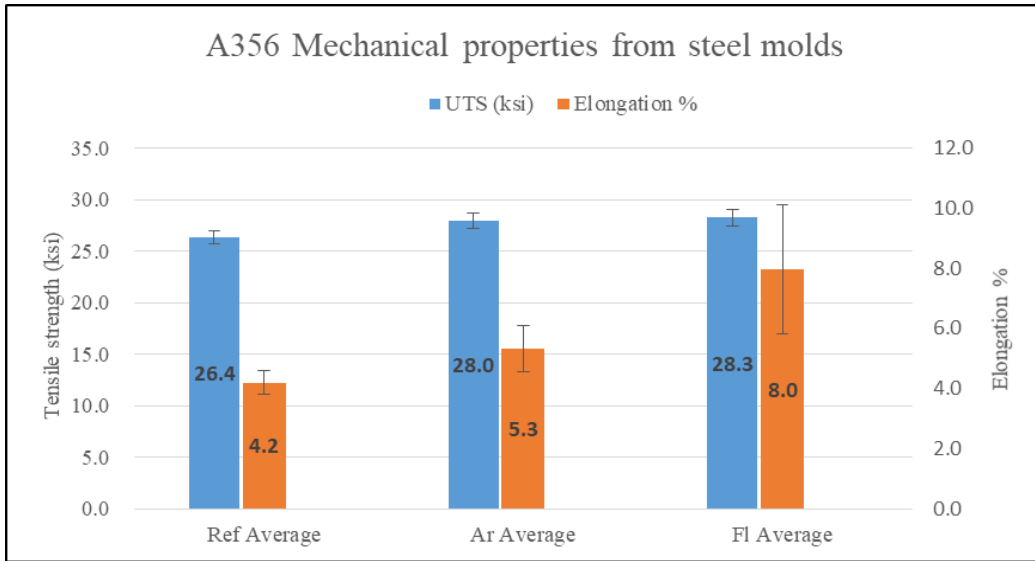


(a)

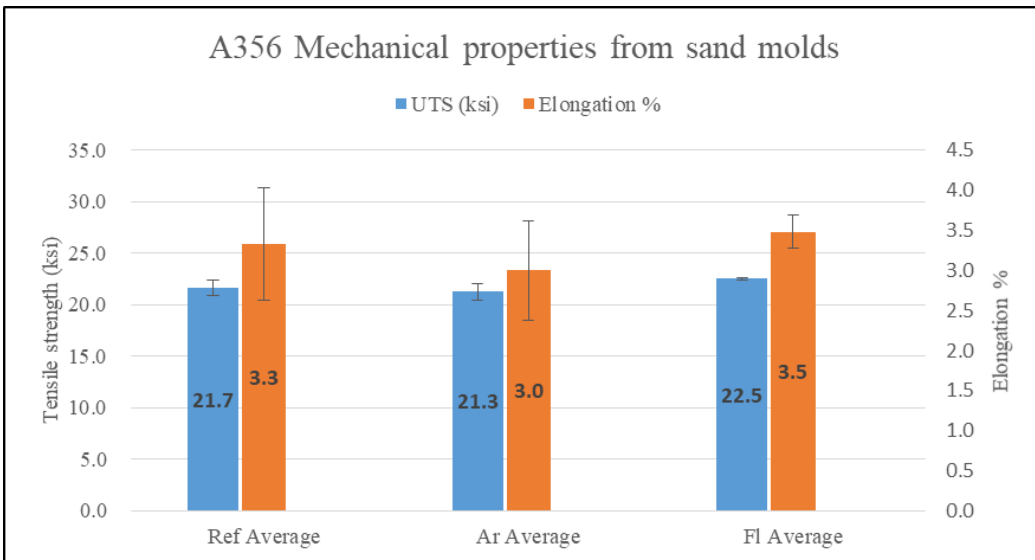


(b)

Figure 6.10. Stress-strain curves of C355 aluminum alloy under different conditions (a) sand mold (b) steel mold

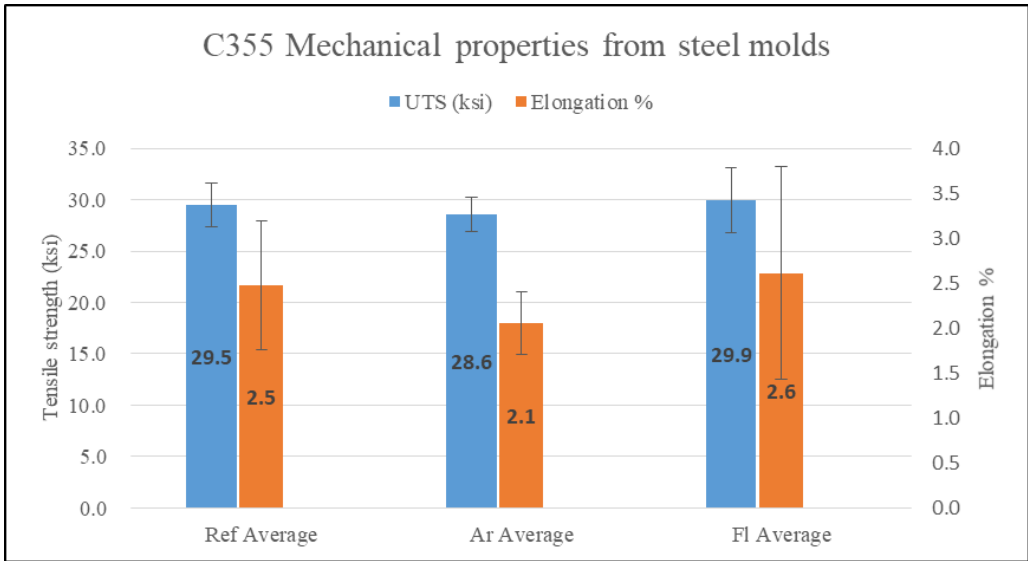


(a)

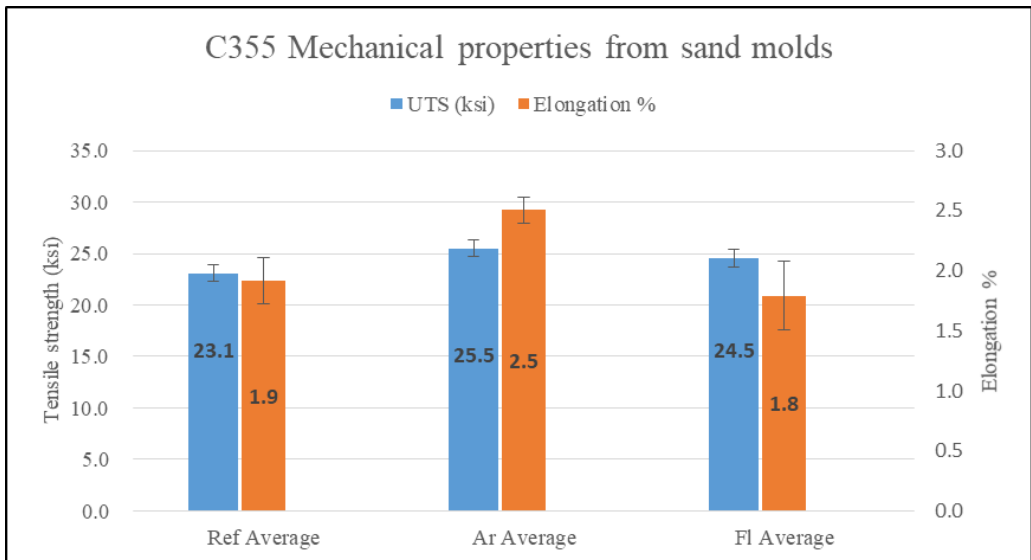


(b)

Figure 6.11. Mechanical properties of A356 aluminum alloy cleaned by different procedures
(a) Steel mold (b) Sand mold



(a)



(a)

Figure 6.12. Mechanical properties of C355 aluminum alloy cleaned by different procedures
 (a) Steel mold (b) Sand mold

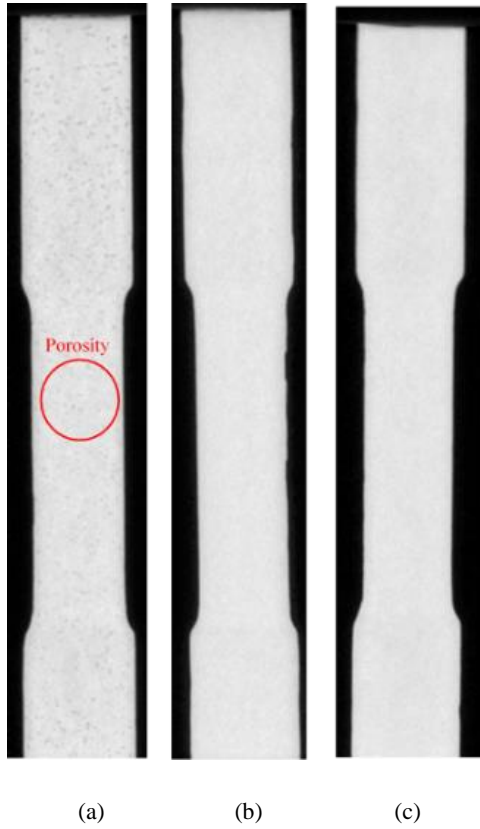


Figure 6.13. CT results of C355 tensile bars from sand molds (a) Reference (b) Argon (c) Flux

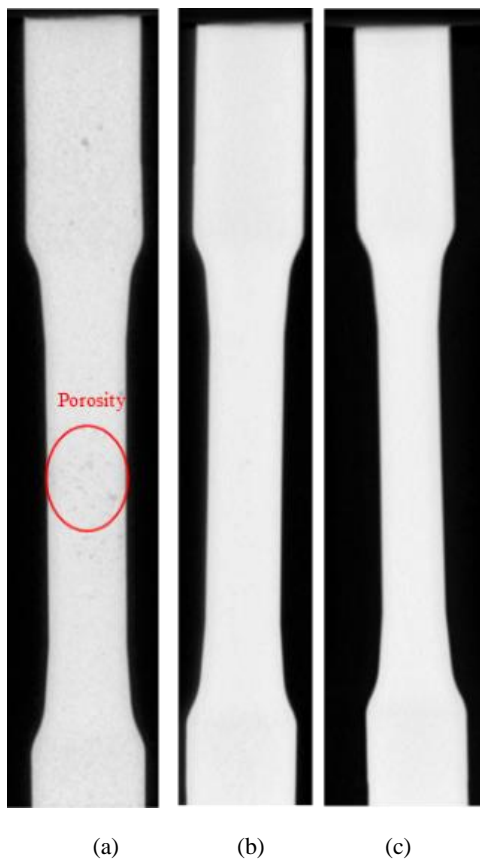


Figure 6.14. CT results of C355 tensile bars from steel molds (a) Reference (b) Argon (c) Flux

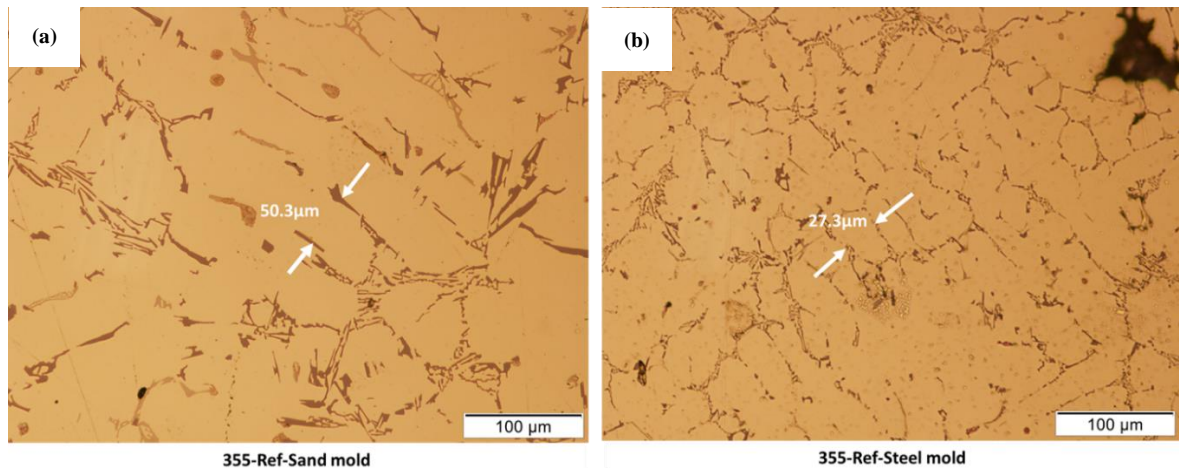


Figure 6.15. Microstructures of C355 samples from different types of molds (a) sand mold (b) steel mold

6.2.4. Fracture surface

Fracture surfaces were provided by the tensile test to figure out if there were any internal defects can be detected. The stereo optical microscope (Nikon SMZ 1500) was used to get the magnified views of each sample's fracture surface. The fracture surfaces of two alloys with different cleaning process from the sand mold and the steel mold are shown in Figure 6.16 and Figure 6.17, respectively. Two samples with the same condition are selected. The right two columns are the photos of C355 aluminum alloy while the left two columns are the photos of A356 aluminum alloy. It is noted that the photos in each row are subjected to the same cleaning process.

To get more details of the fracture surface, the SEM was performed. The analyses of the morphology of C355 aluminum alloys samples from sand and metal mold with different cleaning process were performed by a JEOL JSM-7000F equipped with Oxford Instruments EDS detector. The results are shown in Figure 6.18 and Figure 6.19, respectively. Each row of the figure consists of three images which represent the same position of a sample at different magnifications (750×, 1500×, 3000×).

As seen from Figure 6.16 and Figure 6.17, there is an evident improvement between reference trial and those two trials with cleaning procedures. Although it is hard to find the difference between the fracture surfaces of argon trial and flux trial. And no sign shows that argon trial has better results than the flux trial. Furthermore, as learnt from SEM images, their surface morphologies is quite similar. Both cleavage and dimple exist on their surfaces (see Figure 6.18 and Figure 6.19), indicating that the fracture mechanism is a mixed fracture mode. The presence of a little amount of dimples is accorded with the low ductility of the tensile bars shown in Figure 6.12.

Defects appeared on the surfaces of reference trial are evident, the black area and those white dots occur on the surfaces of the samples from steel molds and the sand molds, respectively. The morphology of the black area is shown in Figure 6.20. It can be seen that this area is filled with the exposed dendrites, which could be the indication of the shrinkage porosity. Moreover, the mapping results of EDS (Figure 6.21) shows the oxides should be the spinel ($MgAl_2O_4$) which form on the dendrites, and this may be the reason for the black color. In order to identify the white dots, the optical microscope micrograph and SEM image at the same position on the surface of the sample from reference trial (Figure 6.22) are compared, it is thought that those white dots on the surface are due to the exposed dendrites without attachment of oxides, which also indicate the effect of shrinkage porosity.

Besides those defects occurred on the samples in the reference trial, the surfaces of samples from steel molds have the characteristic of relatively bright white areas. Figure 6.23 (b) and Figure 6.23 (c) are the morphologies of two positions for the same sample from argon trial. As seen from Figure 6.23 (b), the morphology has the exposed dendrites, which cause the presence of bright white area on the fracture surface, while the regular part of the fracture surface has the regular morphology with the cleavage that shown in Figure 6.23 (c). It should be noted that those exposed dendrites are the indication of the shrinkage porosity. Hence, similar to those white dots on the surface of reference trial sample, the white area can be regarded as the aggregation of a bunch of smaller white dots which represent the existence of the shrinkage inside the sample.

In summary, the defects detected on the fracture surfaces of samples with cleaning procedures are mainly caused by shrinkage, which is a common defect that occurs during casting and it is hard to avoid. These shrinkage porosity can improve the formation of fracture nucleation sites and initial the fracture quickly. Therefore the shrinkage could be one of the reasons that there is no improvement on the mechanical properties after cleaning procedures rather than any defects that are introduced by metal-mold reaction.

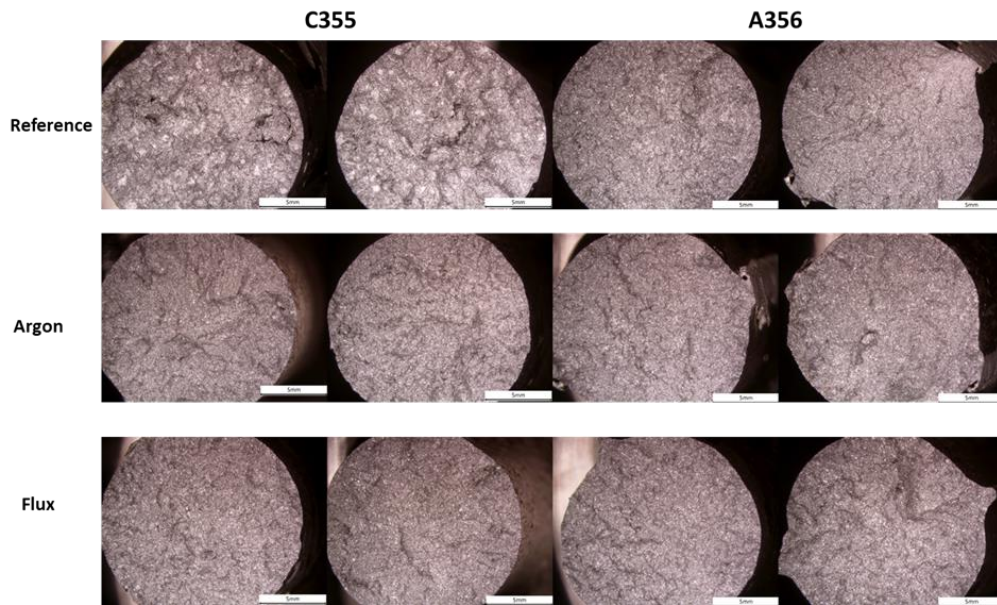


Figure 6.16. The comparison of fracture surface for the C355 and A356 aluminum alloy samples with different cleaning procedures (Sand mold)

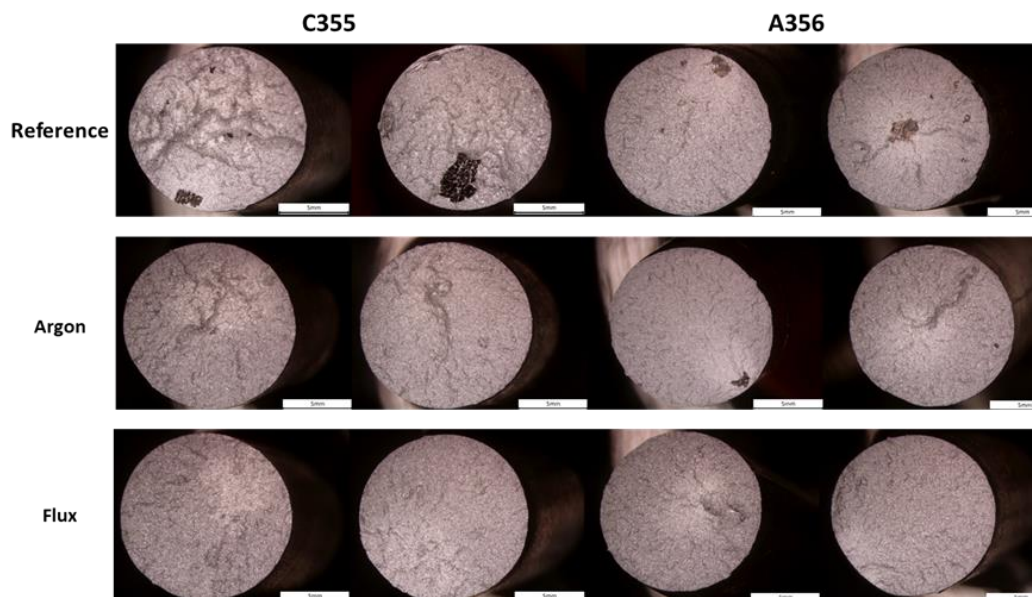
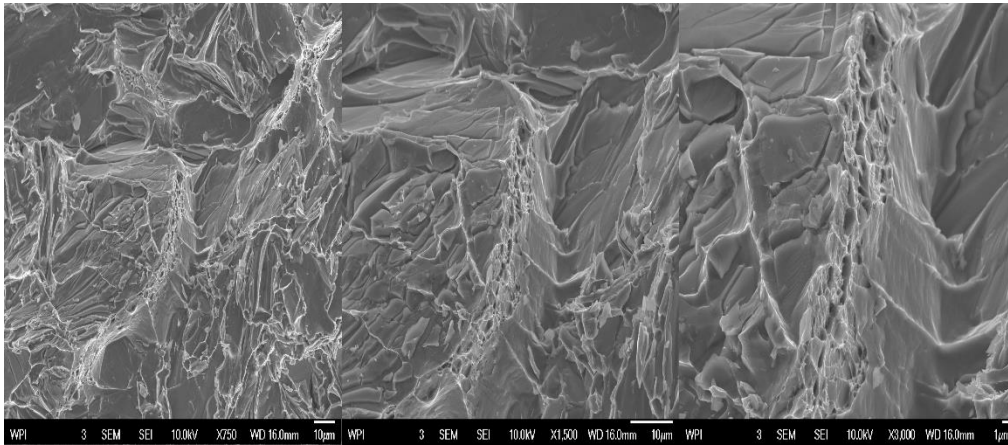
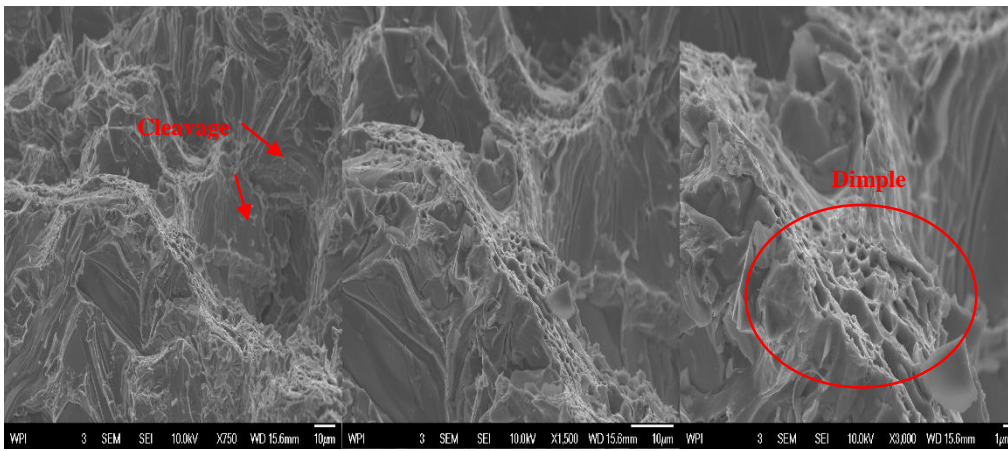


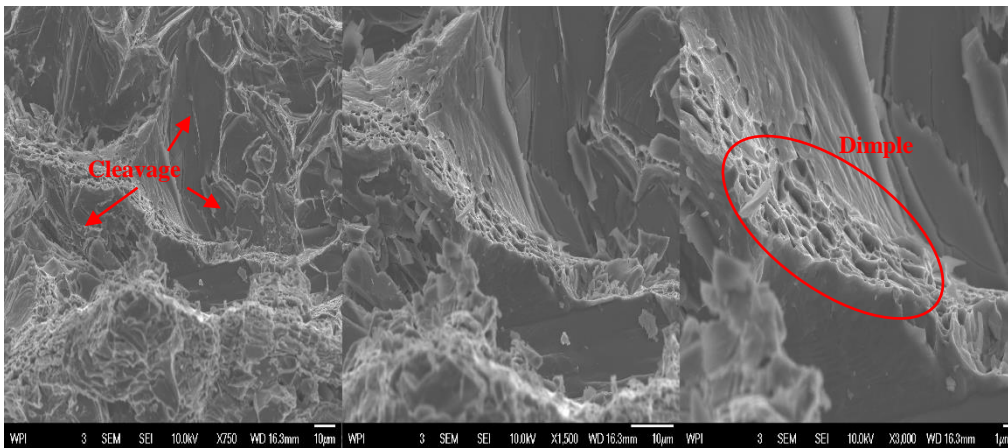
Figure 6.17. The comparison of fracture surface for the C355 and A356 aluminum alloy samples with different cleaning procedures (Steel mold)



(a)

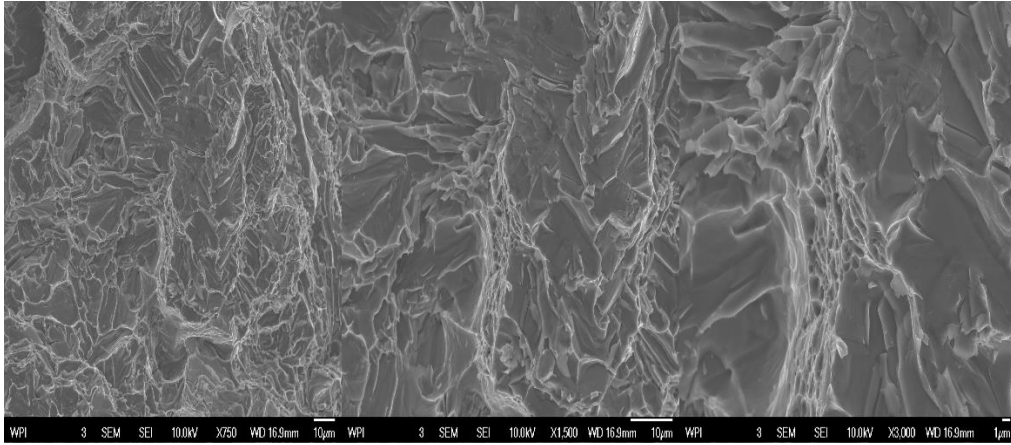


(b)

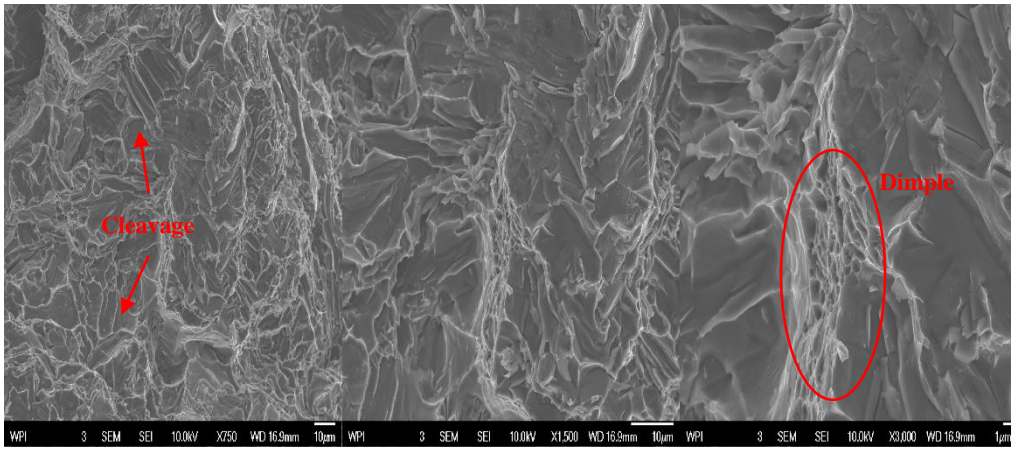


(c)

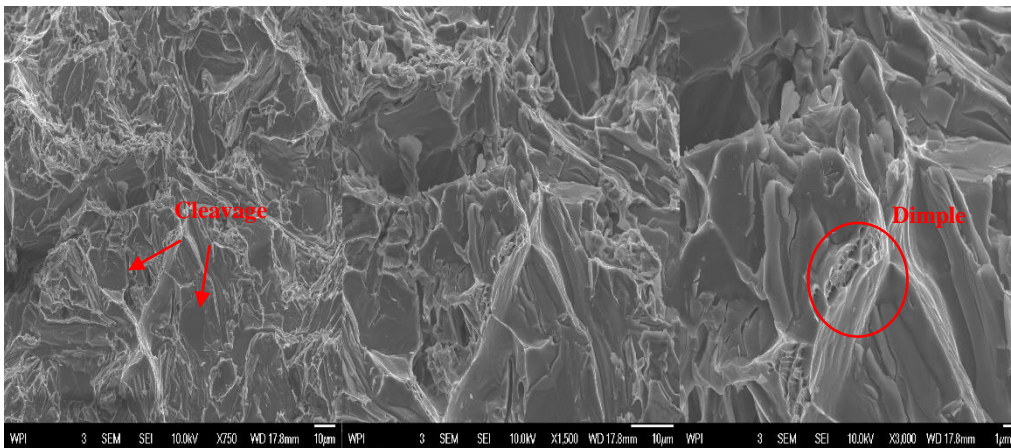
Figure 6.18. Fracture morphology of C355 aluminum alloy sample from sand mold with different cleaning procedures (a) Reference; (b) Argon; (c) Flux



(a)



(b)



(c)

Figure 6.19. Fracture morphology of C355 aluminum alloy sample from steel mold with different cleaning procedures (a) Reference; (b) Argon; (c) Flux

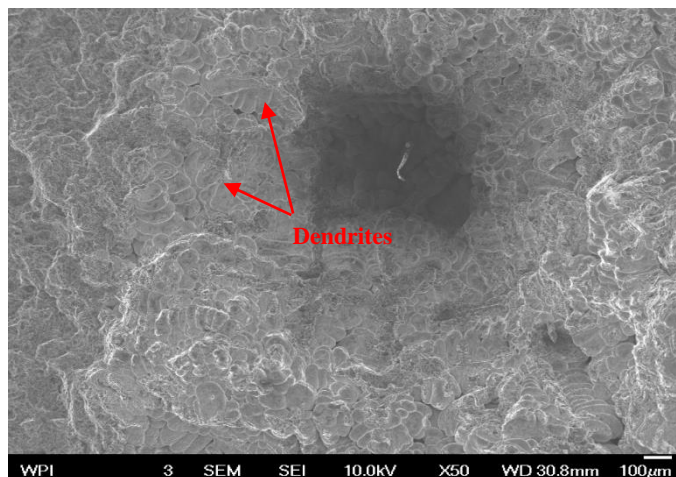


Figure 6.20 Morphology of the black area on the fracture surface

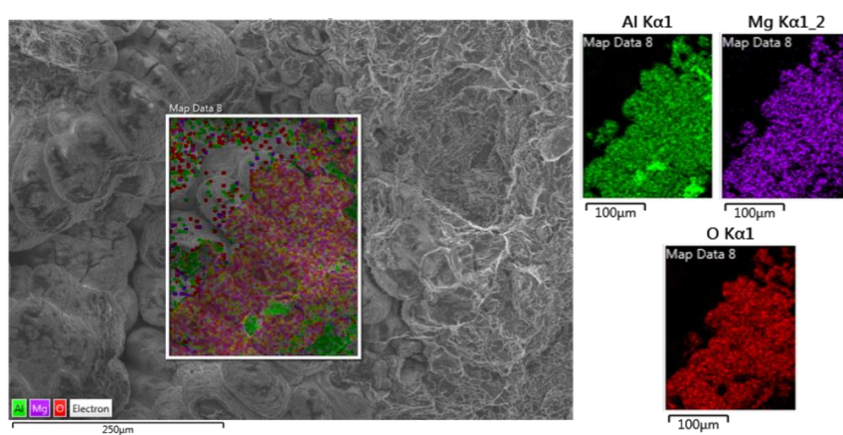


Figure 6.21 Mapping results of the grape-like dendrites on the black area

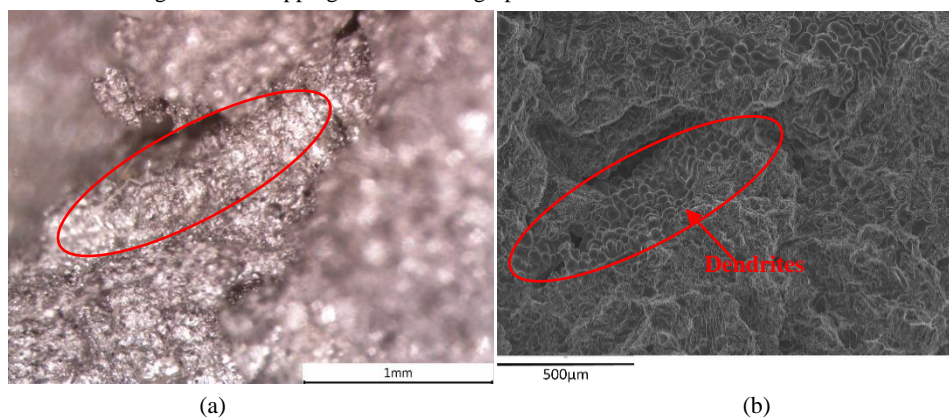
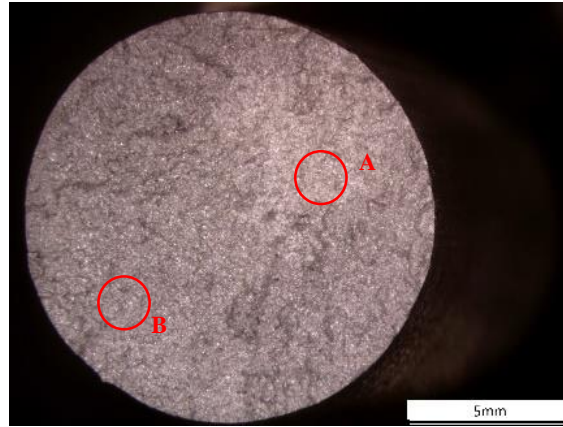
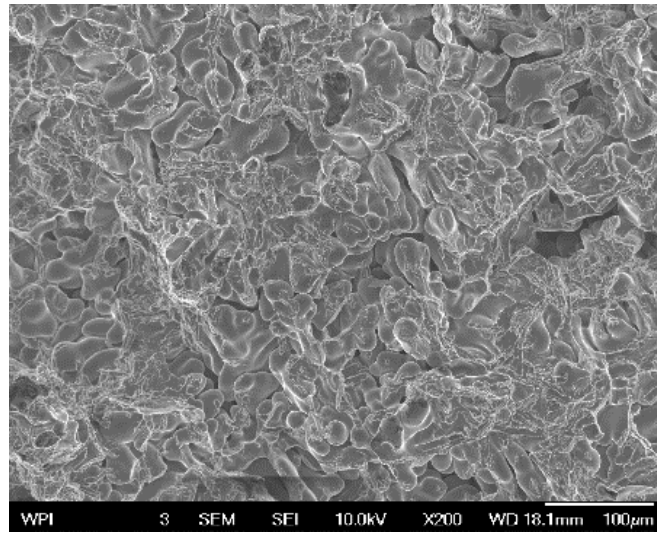


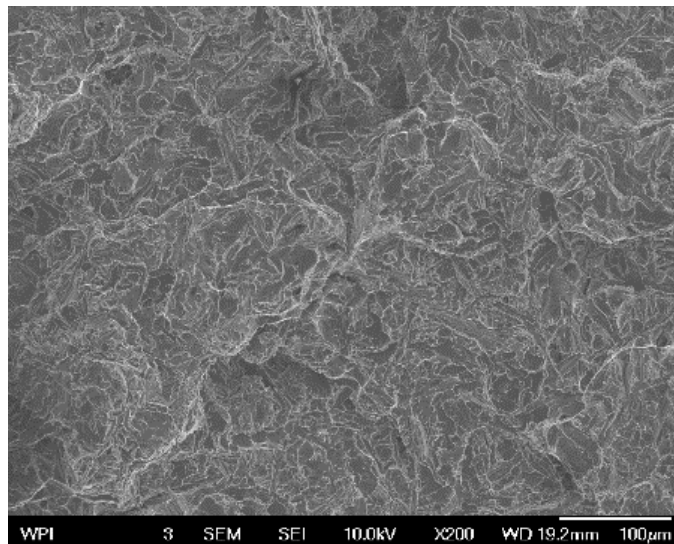
Figure 6.22. Surface morphology of the sample of reference trial; (a) Optical microscope micrograph (b) SEM image at the same position



(a)



(b)



(c)

Figure 6.23 Surface morphology of the sample from the flux trial (a) position A; (b) Position B

6.2.5. Fluidity

The measured results of fluidity with different cleaning procedures are shown in Figure 6.24. Surprisingly, compared with reference trial, the melt with argon degassing has better fluidity, while it seems that the chlorine degassing has no effect on the fluidity.

Previous investigations have confirmed that the fluidity is influenced by melt composition, melt temperature, mold material, melt viscosity and melt cleanliness, etc. [14]. At this case, the melt composition of the same alloy can be regarded as constant. As shown above, cleaning procedures do not change the composition of the melt. The temperature of the melt during the spiral test is held at $1310 \pm 2^\circ\text{F}$, so it is believed that the temperature has no significant impact on the fluidity. Furthermore, all sand molds used in the trial are no-bake sand molds. Thus, the difference of their fluidity could be derived from the cleanliness of the melt, oxides and inclusion, specifically. Crepeau et al [15] and Kwon and Lee [16] have demonstrated that the decrease on inclusions and oxides in the melt can improve the melt fluidity. Based on the results of spiral test, it seems that more oxides or inclusions were left via chlorine degassing than via argon degassing. This phenomenon indirectly proves that internal defects are not caused by argon degassing. On the other hand, it is possible that in industry, with the relatively more complex gating system, it may be easier to form the oxides in the melt with argon degassing, thus resulting in the formation of defects. More researches are needed to determine if there are other factors to affect fluidity.

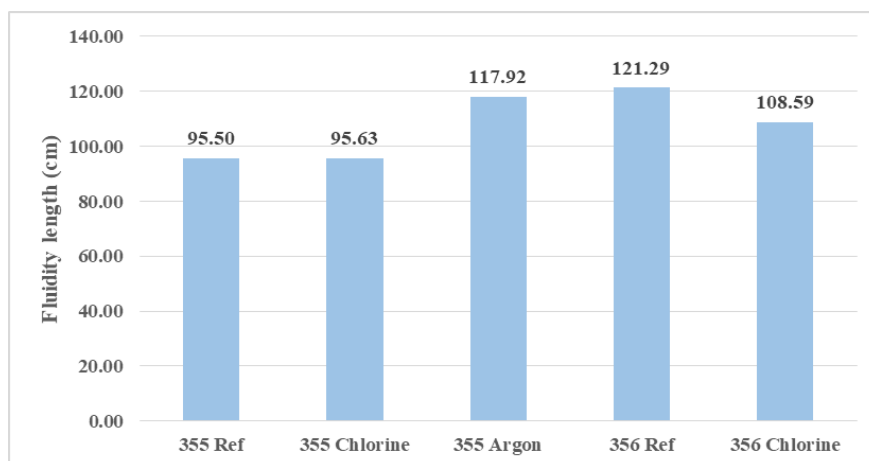


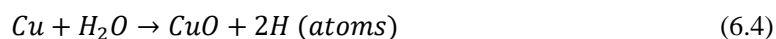
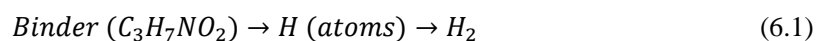
Figure 6.24. Effect of cleaning procedures on melt fluidity

6.3. Surface defects

The average of profile roughness (Ra) of each sample is calculated by the extraction of sample's surface profile. The results of samples with different cleaning procedures are shown in Figure 6.25. For the trials with no-bake sand molds, also shown in the Figure 6.25, the argon trial of C355 aluminum alloy is the most distinct among these trials. It is likely that argon causes the rougher surface during casting. However, the surfaces are much smoother in the trial with green sand mold. Another interesting finding is that generally samples with the same cleaning procedure from no-bake sand molds have rougher surfaces than those from green sand mold and this is also evidently visible (see Figure 6.26). Both the two samples shown in Figure 6.26 are degassed by argon, while the left sample from no-bake sand mold yields more pits and bumps on the surface than that from green sand mold. In fact, besides surface defects, there are other factors that could influence the surface roughness. The type of mold, sample shape, melt temperature etc. are always considered during analyzing the surface roughness of castings. In this case, all samples have the same shapes and the melt temperature are controlled from 1310°F to 1315°F. Thus, surface defects and sand mold type mainly contribute to the variation of surface roughness.

Effect of the type of sand mold

Generally, the chemical binder and molding process are two main differences for these two kinds of molds. Figure 6.27 shows various features on a sample of no-bake sand mold, which indicates the influence from no-bake sand. It is known that no-bake sand can be bonded to form the mold with the addition of chemical binder and the release agents. Once the melt pours into the mold, the organic binder decomposes at high temperature. At this case, the main component in the binder is urethane ($C_3H_7NO_2$). Similar to the iron sand mold casting ^[17] some reactions as follows with the melt may happen at the metal-mold interface:



From these reactions, firstly, the high temperature could decompose the chemical binders and release the atomic hydrogen and oxygen. Then, the hydrogen atoms could aggregate to form hydrogen porosity, and the melt is likely to form the oxides with the oxygen. These defects are left on the surface of the sample and result in the surface unevenness.

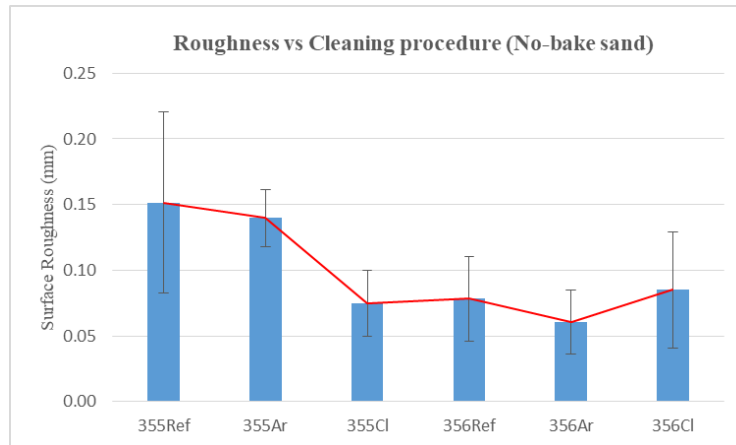
Besides the influence from the binder, the molding process of no-bake sand mold causes the unsmoothness of the surface. During the molding process, unlike the green sand mold which was tightly rammed and compacted by the machine, sand is manually compacted for the no-bake sand mold. Therefore, the voids between sand grains are larger in the no-bake sand mold and the melt can flow into the void and leave a hump on the surface. Furthermore, since the sand is not rammed tightly, some sand grains may scrub from the mold and cause defects.

Effect of the metal-mold reaction

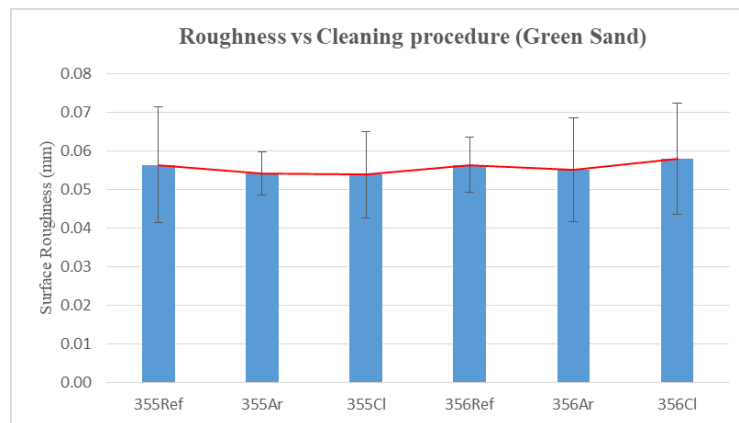
In figure 6.25(a), for C355 aluminum alloys, it can be seen that argon degassing seems ineffective as another cleaning method in which chlorine is used. Two possible reasons for this phenomenon are the usage of argon and the lack of usage of chlorine. The former is less likely to be the point for this problem since argon, which belongs to inert gas, is hard to react with any substances and would not produce any defects. Thus, for C355 aluminum alloy, this ineffectiveness probably relates to the usage of chlorine. Because of the chemical binder shown above in no-bake sand mold, the copper that exists in the melt would form copper oxides. However, as learned from the result reported by Utigard^[18] (see Figure 6.28), with the chlorine in the melt, it is much easier to form copper chloride than copper oxide due to its more negative Gibbs free energy. More copper would form copper chlorides and float on the melt surface during cleaning process and are removed before pouring. The reaction shown in Eq 6.4 could be suppressed, and fewer oxides would be created. Hence, with the argon degassing and lack of the addition of chlorine, the defects caused by oxides tend to form in the no-bake sand mold rather than in the green sand mold. Nevertheless, in green sand mold, without the influence of the binder, the differences between cleaning processes are not significant (Figure 6.25(b)).

In addition, as learned from Figure 6.25, the higher standard deviation of the average surface roughness shows significant change of roughness at different surface positions. According to the thickness of a sample, the measurement planes are extracted from the thin part and the thick part (see Figure 5.16). Figure 6.29 shows the relationship between surface roughness and the thickness of a sample. It can be seen that the surface is rougher at the thinner section of a sample. At the thinner section, the heat transfer is quicker than at the thicker section. Hence the temperature drops more rapid at the thinner section, which indicates that the temperature is lower at the thinner section at the same time after pouring the melt. For the no-bake sand mold, the reactions that forms oxides and other substances are mainly exothermic. According to Le Chatelier's principle, the exothermic reaction can shift to the right when temperature decreases, which give rise to formation of more

oxides and defects. On the other hand, without the binder in the mold, more defects also occur on the thinner section of the sample from the green sand mold.



(a)



(b)

Figure 6.25. Results of profile roughness (a) No-bake sand mold (b) Green sand mold

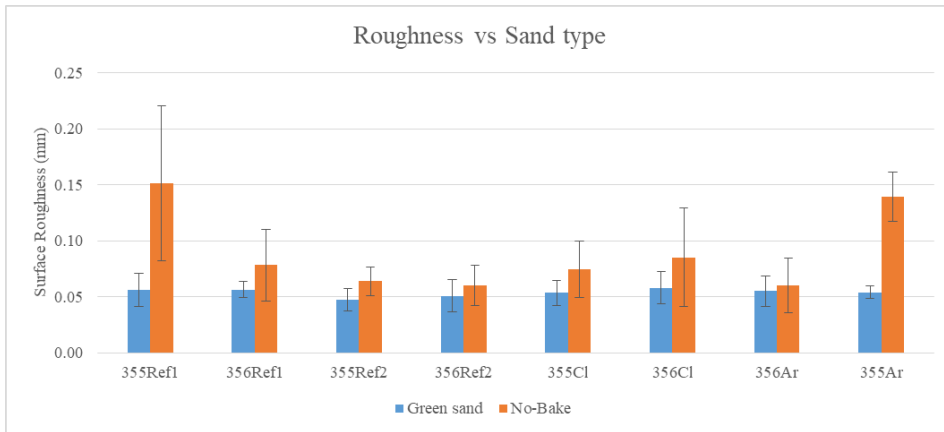


Figure 6.26. Comparison of surface roughness between types of sand mold

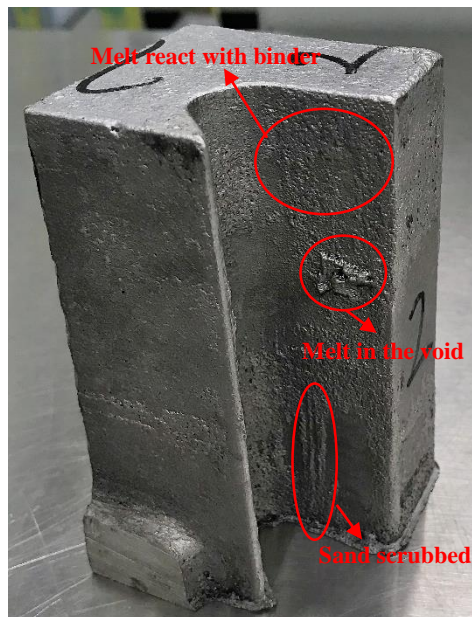


Figure 6.27. Surface defects on the sample

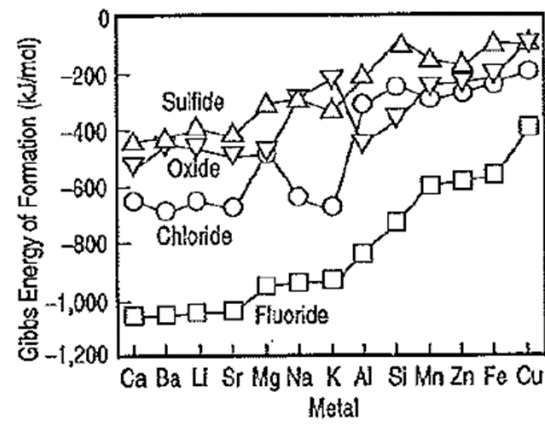


Figure 6.28 Standard Gibbs energy of formation of different substances [18]

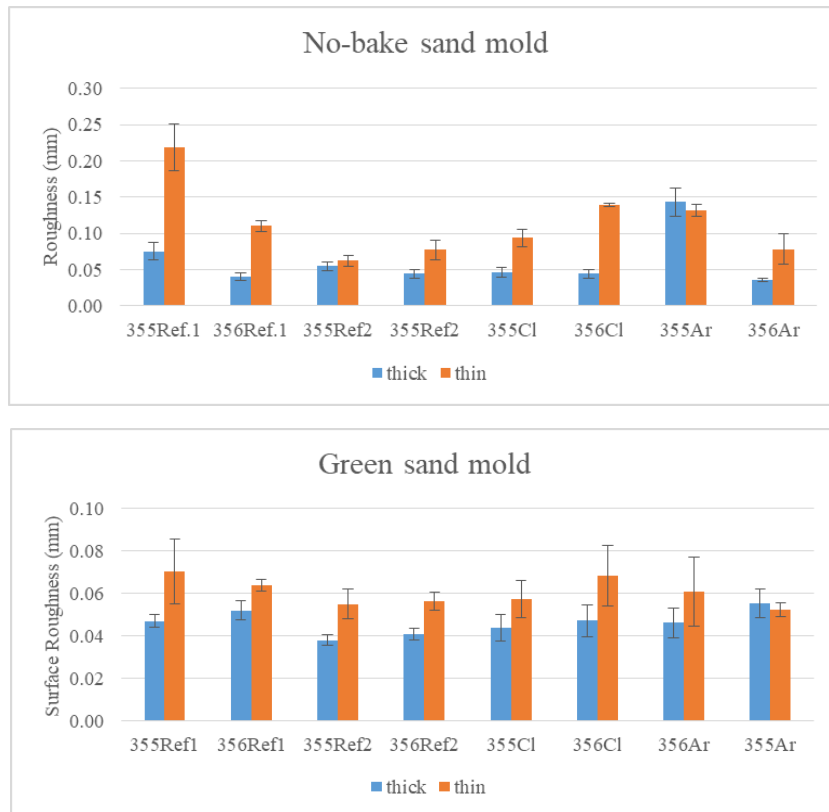


Figure 6.29. Comparison of surface roughness between the thicknesses of sample

7. Conclusion

To develop a new green cleaning method without using chlorine, the origin of defects that occur on the copper containing aluminum alloys with argon degassing were studied and their formation mechanisms were discussed in this work.

Ineffective degassing

- i. Degassing with argon can effectively extract the hydrogen in the molten copper containing aluminum alloys. At the beginning of the degassing, the extraction rate is the highest and the rate decreases as degassing time goes on. After 20 min, further degassing does not decrease the amount of the porosity.
- ii. CT scan with the post-process software can be an effective method to qualitatively and directly evaluate the porosity inside the sample.

Metal-mold reaction

- i. The metal-mold reaction does not influence the mechanical properties of the sample by introducing the internal defects. In the experiments, the lower mechanical properties are mostly caused by the shrinkage porosity.
- ii. The defects occurred on the surface of the sample relate to the type of the sand mold. The chemicals, such as binder and agent that are contained in the no-bake sand are easy to react with the mold and cause the rough surface. Unlike chlorine, the argon cannot suppress the reaction between copper in the melt and the oxygen from the organic binder. Without the binder, in the green sand mold, metal-mold reaction could happen on the sample surface, however, cleaning procedures and alloy types do not contribute to the occurrence defects.
- iii. The fluidity difference among the different cleaning procedures does not contribute to the occurrence of defects.

Besides the work that has been performed at present, more work is needed to figure out the reason for the origin of defects. Some recommendations are listed below:

- i. Oxides that are produced during casting could be the reason for the defects. These oxides could be caused by the turbulence in the gating system. Hence, the shape of gating system could be a focus in the future work.
- ii. Apply the LIBS and PoDFA to analyze the melt with different cleaning procedures so that the level of oxides can be determined.
- iii. The alloy with higher copper content (A206) can be used in the further experiments

Reference:

- [1] Davis, J.R. (1998). *Metals Handbook, Desk Edition (2nd Edition) - 41.1. The Aluminum Industry*. ASM International.
- [2] Han, Q., and S. Viswanathan. "Hydrogen evolution during directional solidification and its effect on porosity formation in aluminum alloys." *Metallurgical and Materials Transactions A* 33.7 (2002): 2067-2072.
- [3] Wriedt, H. A. "The Al– N (Aluminum-Nitrogen) system." *Bulletin of Alloy Phase Diagrams* 7.4 (1986): 329-333.
- [4] Gilbert KJ, L RE. *The Influence and Control of Porosity and Inclusions in Aluminum Castings*. In: ASM International; 2004
- [5] Zhao, L., Pan, Y., Liao, H., Wang, Q., & Zhao, L. (n.d.). Degassing of aluminum alloys during re-melting. *Materials Letters*, 66(1), 328–331.
- [6] Neff DV. Understanding aluminum degassing. *Modern Casting*. 2002; 92 (5):24-6.
- [7] Degassing: Degassing of Aluminum Alloys. In: ASM International; 2008
- [8] Wu, R., Qu, Z., Sun, B., Shu, D., & Wu, R. (n.d.). Spray Degassing as a Method for Hydrogen Removal in Aluminum Melts. *Materials Transactions*, 48(5), 1029–1033.
- [9] Xu H, Han Q, Meek T T. Effects of ultrasonic vibration on degassing of aluminum alloys [J]. *Materials Science and Engineering: A*, 2008, 473(1-2): 96-104.
- [10] Zolotarevsky, Vadim S. Belov, Nikolai A. Glazoff, Michael V.. (2007). *Casting Aluminum Alloys - 1.1 The Role of Alloying Elements and Dopants: Basic Alloy Systems*.
- [11] Ye, Haizhi. "An overview of the development of Al-Si-alloy based material for engine applications." *Journal of Materials Engineering and Performance* 12.3 (2003): 288-297
- [12] Caceres, C. H., et al. "The effect of Cu content on the level of microporosity in Al-Si-Cu-Mg casting alloys." *Scripta Materialia* 40.5 (1999): 631-637.
- [13] Gadelmawla ES, Koura MM, Maksoud TMA, Elewa IM, Soliman HH. Roughness parameters. *Journal of Materials Processing Technology*. 2002; 123(1):133-45.
- [14] Di Sabatino, Marisa. "Fluidity of aluminium foundry alloys." (2005).
- [15] P. N. Crepeau, M. L. Fenyas, J. L. Jeanneret, *Modern Casting* (1992) 28-30
- [16] Y., Lee, Z., & Kwon, Y. (n.d.). The effect of grain refining and oxide inclusion on the fluidity of Al-4.5Cu-0.6Mn and A356 alloys. *Materials Science and Engineering A*
- [17] Naro, R. (n.d.). Porosity in Iron Castings from Mold-Metal Interface Reactions. *Modern Casting*, 90(4), 41–44
- [18] T. A. Utigard, in: *Proceedings of the International Symposium on Extraction, Refining, and Fabrication of Light Metals* (Ottawa, Canada: CIM, 1991), p. 353

